Brain, Behavior, and Immunity 117 (2024) 493–509

Contents lists available at ScienceDirect

Brain Behavior and Immunity

journal homepage: www.elsevier.com/locate/ybrbi

Loss of interleukin 1 signaling causes impairment of microglia- mediated synapse elimination and autistic-like behaviour in mice

Antonella Borreca [a,b], Cristina Mantovani [b,c,1], Genni Desiato [b,1], Irene Corradini [a,b], Fabia Filipello [b], Chiara Adriana Elia [b,2], Francesca D'Autilia [b], Giulia Santamaria [b], Cecilia Garlanda [b,c], Raffaella Morini [b], Davide Pozzi [b,c,*], Michela Matteoli [a,b,*]

[a] Institute of Neuroscience (IN-CNR), Consiglio Nazionale delle Ricerche, Milan, Italy
[b] IRCCS Humanitas Research Hospital, Via Manzoni 56, 20089 Rozzano, Milan, Italy
[c] Department of Biomedical Sciences, Humanitas University, Via Rita Levi Montalcini 4, 20072 Pieve Emanuele, Milan, Italy

ARTICLE INFO

Keywords:
Proinflammatory cytokines
IL-1 signaling
Interleukin-1 Receptor antagonist (IL-1Ra)
Autism spectrum disorder (ASD)
Synaptic density
Microglia
Synapse engulfment
mTOR signaling
Rapamycin treatment
Neurodevelopmental disorders

ABSTRACT

In the last years, the hypothesis that elevated levels of proinflammatory cytokines contribute to the pathogenesis of neurodevelopmental diseases has gained popularity. IL-1 is one of the main cytokines found to be elevated in Autism spectrum disorder (ASD), a complex neurodevelopmental condition characterized by defects in social communication and cognitive impairments. In this study, we demonstrate that mice lacking IL-1 signaling display autistic-like defects associated with an excessive number of synapses. We also show that microglia lacking IL-1 signaling at early neurodevelopmental stages are unable to properly perform the process of synapse engulfment and display excessive activation of mammalian target of rapamycin (mTOR) signaling. Notably, even the acute inhibition of IL-1R1 by IL-1Ra is sufficient to enhance mTOR signaling and reduce synaptosome phagocytosis in WT microglia. Finally, we demonstrate that rapamycin treatment rescues the defects in IL-1R deficient mice. These data unveil an exclusive role of microglial IL-1 in synapse refinement *via* mTOR signaling and indicate a novel mechanism possibly involved in neurodevelopmental disorders associated with defects in the IL-1 pathway.

1. Introduction

Autism spectrum disorder (ASD) is a neurodevelopmental disorder characterized by impaired social abilities and repetitive behavior that affects at least 1% of the population. More than one hundred genes have been linked to ASD, involving rare and common genetic variants, each contributing to a low risk to the phenotype (Lim et al., 2013;Yu et al., 2023; Loureiro et al., 2021; Bruel et al., 2022; Rodriguez-Gomez et al., 2021). The genes associated with ASD largely converge on common pathways consistently intersecting at the synapse and potentially affecting its formation, elimination and plasticity (for reviews see Basilico et al., 2020; De Rubeis et al., 2013; Huguet et al., 2013; Satterstrom et al., 2020; Won et al., 2013). Consistently, one of the major features of ASD brains is the excessive spine density in frontal, temporal, and parietal lobes (Hutsler & Zhang, 2010; Pagani et al., 2021; Bourgeron, 2009; Kim et al., 2011). This abnormality was proposed to result from a defect in supernumerary synapse elimination (Tang et al., 2014), a physiological process that provides a selection of synapses and neural circuits in the juvenile postnatal period (Schafer et al., 2012). In line with this view, defects in synapse elimination during development have been shown to be associated with altered synaptic connectivity and autistic-like behaviors (Filipello et al., 2018).

Besides the genetic contribution (Sandin et al., 2014; Tick et al., 2016), environmental risk factors, such as prenatal immune challenges, contribute to the pathogenesis of ASD (Patterson, 2011; Hsiao & Patterson, 2011; Atladóttir et al., 2010; Estes & McAllister, 2015; Ravaccia & Ghafourian, 2020; Mirabella et al., 2021; Corradini et al., 2018; Matteoli et al., 2023). Clinical evidence reported, in ASD subjects, alterations in proinflammatory cytokines (Hall et al., 2023; Boccazzi et al., 2023), and, among these, interleukin-1β (IL-1β) (Estes & McAllister,

* Corresponding authors at: Department of Biomedical Sciences, Humanitas University, Via Rita Levi Montalcini 4, 20072 Pieve Emanuele, Milan, Italy.
E-mail addresses: davide.pozzi@hunimed.eu (D. Pozzi), michela.matteoli@hunimed.eu (M. Matteoli).
[1] Equal contributors.
[2] Current address: Institute of Neuroscience (IN-CNR), Consiglio Nazionale delle Ricerche, Milan, Italy.

https://doi.org/10.1016/j.bbi.2024.01.221
Received 5 October 2023; Received in revised form 11 January 2024; Accepted 25 January 2024
Available online 1 February 2024

2015). ASD is indeed associated with genes for IL-1β, its receptor (IL-1R1), and receptor-associated protein family, including the IL-1β decoy receptor IL-1 receptor type 2 (IL-1R2) (O'Roak et al., 2011; Sanders et al., 2012) and the interleukin-1 receptor accessory protein-like 1 (IL1R1APL1) (Piton et al., 2008). Polymorphisms of the interleukin-1β genes were found to be more frequent in children with ASD (Saad et al., 2020). Several groups reported higher IL-1 levels in ASD children and skewed IL-1β responses following stimulation (Ashwood et al., 2011; Suzuki et al., 2011; reviewed in Zhao et al., 2021). Also, compared to controls, monocytes from children with ASD were found to produce excessive IL-1β following LPS exposure (Jyonouchi et al., 2001; Enstrom et al., 2010). However, other studies failed to detect changes in IL-1 levels in ASD subjects (Vargas et al., 2005; Xiao-Jing Li , 2009). Some groups even found that the IL-1R antagonist, IL-1Ra -which dampens IL-1 signaling- is significantly increased in ASD (Suzuki et al., 2011; Saad et al., 2020), and decreased levels of IL-1β were associated with increased severity of presentation of the disease in females (Masi et al., 2017). Thus, data concerning the cytokine involvement in ASD are still rather controversial.

IL-1β plays an endogenous role in the brain. Expression of the cytokine (Giulian et al., 1988; Breder et al., 1988; Lechan et al., 1990) and its receptor (IL-1R) (French et al., 1999; Iwamasa, 1997; (Hewett et al., 2012) was demonstrated in basal conditions during CNS development. Physiological concentrations of IL-1 play a neuromodulatory role in neuronal ion channels, cell excitability and neuroplasticity (O'Connor & Coogan, 1999, Viviani et al., 2007, Schäfers & Sorkin, 2008). In particular, IL-1β is induced in the hippocampus during learning processes and is critical for maintenance of long-term potentiation (LTP) (Ross et al., 2003). Furthermore, the upregulation of IL-1Ra, which dampens the cytokine signaling, negatively impacts synaptic plasticity, memory consolidation and behavior, suggesting that the cytokine endogenously acts in the CNS to perform non-immunological functions necessary for proper brain function (Spulber et al., 2011, Goshen et al., 2007).

Based on these observations as well as on the observation that endogenous levels of immune molecules regulate sociability and cognitive functions (Filiano et al., 2016; Herz et al., 2021), two domains strongly impaired in ASD, we aimed to assess whether not only the enhancement but even the downregulation of IL-1 signaling may contribute to ASD features. Using a combination of genetic and pharmacological manipulation of the IL-1 pathway, we demonstrate that the lack of cytokine signaling in mice leads to impairment of synapse engulfment by microglia and autistic-like phenotype, as a result of mTOR deregulation.

2. Material and methods

2.1. Animals

Il1r1$^{-/-}$ (Jackson Laboratories, Bar Harbor. B6.129S7-*Il1r1*^{tm1Imx} J. Strain #:003245. (Percie du Sert et al., 2020; Glaccum et al., 1997) and WT (C57BL/6) mice were used for the following procedure. *Il1r1*$^{-/-}$ were prepared as follows in C57BL/6 background. A neomycin resistance cassette replaced two exons of the gene, which encode amino acids 4 – 225 of the mature protein. A null mutation in *Il1r1* was generated by homologous recombination in 129/SvEv AB1 ES cells using a replacement vector in which a 2.4 kb EcoR1-Pst1 fragment encompassing two exons was replaced with a PGKneo cassette. Mice homozygous for the *Il1r1*^{tm1Imx} targeted mutation therefore fail to respond to IL-1 and exhibit an altered immune response to many different target proteins. Mice were housed in an air-conditioned room (23 ± 1°C), with food and water ad libitum. The behavioral experiments were conducted during the first half of the dark phase of the 12-h light/dark cycle. Primary hippocampal cultures were performed from E17 embryos while microglia primary cultures were obtained from P1-3 animals. Tissues for Western Blot and RNA analysis were taken from P20, 1 month- 3 months- and 7 months-old male animals. All the experimental procedures followed the guidelines established by the European Legislation (Directive 2010/63/EU), and the Italian Legislation (L.D. no 26/2014). All experiments were conducted according to ARRIVE 2.0 guidelines (Percie du Sert et al., 2020).

2.2. Drugs and treatments

2.2.1. In vitro treatment

For *in vitro* experiments, the following drugs were used: IL-1Ra 100 ng/ml for 24 h (Tomasoni et al., 2017); rapamycin 20 nM for 24 h (Tomasoni et al., 2017), LPS 0.1 μg/mL for 1 h (Lively & Schlichter, 2018).

2.2.2. In vivo treatment

For rapamycin treatment *in vivo*, the protocol was described previously (Sato et al., 2023).

Rapamycin (LC Laboratories, Woburn, MA, USA) was dissolved in 10% dimethyl sulfoxide diluted with saline to 10 mL/kg. The P20 mice received the rapamycin solution (5 mg/kg) or an equal volume of vehicle by intraperitoneal injection once/day for 2 consecutive days. The behavioral tests and brain collection were performed 24 h after the second administration. For brain collection mice were anesthetized and then perfused with saline (NaCl 0,9%) for engulfment analysis. The brain was removed, half brain was post-fixed in PFA 4% overnight at 4°C and half brain underwent hippocampi and cortices dissection for subsequent Western Blot analysis.

2.3. Neuronal cultures

Mouse hippocampal neurons were established from hippocampi at embryonic stage E17 or postnatal 1–2 day-old pups as described previously (Mirabella et al., 2021) with slight modifications. Neurons were plated onto glass coverslips coated with poly-L-lysine at density of 8x10^4 cells. The cells were maintained in Neurobasal medium (Invitrogen) with B27 supplement and antibiotics, 2 mM glutamine and glutamate. All experiments were performed at 13–15 days *in vitro* (DIV). To visualize neuronal processes and dendritic spines, hippocampal neurons were transfected using Lipofectamine 2000 at DIV11 with CAG-GFP plasmid.

2.4. Electrophysiology recording of neuronal cultures

Patch-clamp recordings in neuronal cultures were performed as previously described (Mirabella et al., 2021). In brief, glutamatergic basal synaptic transmission was recorded using the following extracellular solution (in mM): 130 NaCl, 5 KCl, 1.2 KH2PO4, 1.2 MgSO4, 2 CaCl2, 25 HEPES, and 6 Glucose, pH 7.4, in the presence of bicucullin (20 μM), APV (50 μM) and tetrodotoxin (TTX; 1 mM). Glass pipettes of 4–6 MΩ as recording electrodes were filled with the following internal solution (in mM): 135 K-gluconate, 5 KCl, 2 MgCl2, 10 HEPES, 1 EGTA, 2 ATP, 0.5 GTP, pH 7.4. mEPSCs were recorded at − 70 mV as holding potential. The analysis of mEPSC was performed with Mini analysis (Synaptosoft Inc., Fort Lee, NJ, USA).

2.5. Microglial cultures

Primary microglia cell cultures were obtained from mixed cultures prepared from the hippocampi and cerebral cortices of mice at Postnatal day/P1-3. After 14 days of microglia preparation, cells were isolated by shaking flasks for 1 h at 230 rpm. Cells were then seeded on poly-L-ornithine (Sigma) pre-coated wells at a density of 1.5x10^5 cell/mL in DMEM containing 20% heat-inactivated Fetal Bovine Serum (FBS). For microglia-to-neuron co-culture experiments, WT or *Il1r1*$^{-/-}$ microglia were added to hippocampal neurons (13–14 DIV) for 24 h with the ratio of microglia 1.5 : neuron 1. To visualize neuronal processes and

dendritic spines, hippocampal neurons were transfected using Lipofectamine 2000 at DIV11 with CAG-GFP plasmid.

2.6. Phagocytosis assays in vitro

Synaptosome purification and engulfment assay: Synaptosomes were purified as previously described (Huttner et al., 1983) and conjugated with FM1-43FX dye in HBSS at 4°C for 2 min (modified from Biesemann et al., 2014). Unbound FM1-43FX dye was washed out with multiple rounds of centrifugation. WT or *Il1r1*$^{-/-}$ microglia, plated at a density of 1.5x10^5 cells/mL, were then incubated with the same amount of FM1-43FX dye-conjugated synaptosomes for 24 hr. To check the same amount of protein, synaptosomes were quantified by BCA methods and loaded on acrylamide gel. Synaptosomes isolation was checked by synaptic marker measurement (PSD95 and synaptophysin) (data not shown).

2.7. Immunofluorescence

Young (1 month) and old (7 months) animals were used for the analysis of synaptic markers, vGluT1 and PSD95 or the myeloid cell marker Ionized Calcium-Binding Adapter molecule 1 (IBA1) positive cells, and 1-month old animals were used for IL-1R1 staining. Mice were anesthetized with a cocktail of ketamine (100 mg/kg)/xylazine (20 mg/kg) and perfused with 0.9% saline, followed by 4% paraformaldehyde (PFA). Mice were transcardially perfused with 0,9% saline followed by PFA 4%. Brains were rapidly removed and underwent PFA post-fixation overnight. After 24 h brains were left in sucrose 30% diluted in PBS 1X. 50 μm-thick slices were immunostained as follows. Sections at the level of the dorsal hippocampus were blocked at Room Temperature in 10% Normal Goat serum 0.2% Triton X-100 for 45 min or 1% BSA 0.3% Triton X-100 for 30 min and then incubated overnight with specific primary antibodies PSD95 (1:200, Millipore); vGLUT1 (1:1000, SySy) IBA1 (1:400 Wako) (Filipello et al., 2018) or IL-1R1 (1:100, Invitrogen) (Ren et al., 2022), followed by incubation with secondary antibodies (1:400, Alexa Fluor-conjugated, Invitrogen), counterstained with Hoechst and mounted in Fluorosave (Calbiochem). Images were acquired with a SP8II laser scanning confocal microscope (Leica Microsystems), provided with 63X magnification. Images were acquired in the pyramidal layer or stratum radiatum of the CA1 subfield of the hippocampus, as indicated.

2.8. In vivo microglia morphology

Z-stack confocal images were acquired with the SP8II laser-scanning confocal microscope. Images were acquired in the pyramidal layer or stratum radiatum of the CA1 subfield of the hippocampus. For microglial cell count and morphologic analysis, confocal images for the selected marker IBA1 were modified as 8-bit and Z-stack projection images. IBA1 and DAPI^{+} cells were counted per HPF. The resulting images were smoothly processed, binarized and skeletonized, using the Skeletonize Plugin for ImageJ (Arganda-Carreras et al., 2010). Before quantification, a mask using the particle analysis function was created to subtract from skeletonized images. The resulting images were processed by choosing the Analyze Skeleton 2D 3D option in the Skeletonize Plugin, and the number of branches and junctions per cell were obtained.

2.9. In vivo synapse engulfment quantification

Fixed brain slices from WT and *Il1r1*$^{-/-}$ littermates were permeabilized for 45 min at RT in 0.5% Triton X-100, followed by 1 hr RT blocking in 2% BSA 0.5% Triton X-100 and overnight incubation with primary antibody against PSD95 (1:100, Millipore), CD68 (1:400, Bio-Rad) and IBA1 (1:600, Wako) at 4°C. Upon washing, sections were incubated for 2 h at Room Temperature with Alexa-fluorophore-conjugated secondary antibodies (1:400, Invitrogen). Confocal microscopy was performed with a TCS-SP8II Laser Scanning microscope (Leica Microsystems). System, by using a Leica HCX PL APO 63X/ NA 1.3, glycerol-immersion lens. Images were acquired with 3X digital zoom, as 61.5 mm x 61.5 mm in XY, and with a Z-step size of 0.33 μm. Stacks ranged from 5 to 6 μm in thickness. Images were processed and analyzed by Imaris Software (Bitplane, Switzerland) according to the protocol described previously (Schafer et al., 2014). CD68 and IBA1 volumes were quantified by applying 3D surface rendering of confocal stacks in their respective channels, using identical settings (fixed thresholds of intensity and voxel) within each experiment. Each confocal acquisition contained an equal number of WT and *Il1r1*$^{-/-}$ images. For quantification of PSD95 engulfment by microglia, only PSD95 puncta present within microglial CD68^{+} structures were considered. This procedure was used to ensure that only puncta entirely phagocytized by microglia were included in the analysis. To this aim, a new channel for "engulfed PSD95" was created, by using the mask function in Imaris, masking the PSD95 signal within CD68^{+} structures. Quantification of volumes for "engulfed PSD95 in CD68" was performed following the "3D Surface rendering of engulfed material" protocol, previously published by Schafer et al., 2014. To account for variations in cell size, the amount of "engulfed PSD95 in CD68" was normalized to the total volume of the phagocyte (given by IBA1^{+} total volume). The total PSD95 volume per field from the same confocal stacks was also quantified following the same protocol. All the data were normalized to WT values within each experiment.

2.10. Electrophysiology recording of brain slices

Electrophysiological recording in acute brain slices was performed as previously reported (Mirabella et al., 2021). WT and *Il1r1*$^{-/-}$ male mice at P20 were deeply anesthetized with isofluorane at 4% by inhalation and decapitated. Brains were removed and placed in an ice-cold solution containing the following (in millimolar): 87 NaCl, 21 NaHCO3, 1.25 NaH2PO4, 7 MgCl2, 0.5 CaCl2, 2.5 KCl, 25 D-glucose, and 7 sucrose, equilibrated with 95% O2 and 5% CO2 (pH 7.4). Coronal slices (300 μm thick) were cut with a VT1000S vibratome (Leica Microsystems). Slices were incubated at room temperature for at least 1 h, in the same solution as above, before being transferred to the recording chamber. During experiments, slices were superfused at 2.0 mL/min with artificial cerebrospinal fluid (ACSF) containing the following (in millimolar): 135 NaCl, 21 NaHCO3, 0.6 CaCl2, 3 KCl, 1.25 NaH2PO4, 1.8 MgSO4, and 10 D-glucose, aerated with 95% O2 and 5% CO2 (pH 7.4). Cells were examined with a BX51WI upright microscope (Olympus) equipped with a water immersion differential interference contrast (DIC) objective and an infrared (IR) camera (XM10r Olympus). Neurons were voltage (or current) clamped with a Multiclamp 700B patch-clamp amplifier (Molecular Devices, Union City, CA) at room temperature. Low-resistance micropipettes (2–3 MΩ) were pulled from borosilicate. Experiments where series resistance did not remain below 20 MΩ were discarded. Signals were low-pass filtered at 2 kHz, sampled at 10 kHz and analyzed with Digidata 1440A (Molecular Devices). Synaptic basal transmission was recorded at −70 mV respectively in the presence of 1 μM TTX, using the following pipette internal solution (in mM): 138 Cs-gluconate, 2 NaCl,10 HEPES, 4 EGTA, 0.3 Tris-GTP and 4 Mg-ATP (pH 7.2).

2.11. Microglia isolation from hippocampi and cortices and facs analysis

Microglia isolation from hippocampi and cortices from WT mice at P20 and P90 was carried out as previously described (Bennett et al., 2016) with some modifications. The whole procedure was done on ice with cold buffers and centrifuges at 4°C. Anesthetized mice were transcardially perfused using ice cold Hank's balanced salt (HBSS). Hippocampi and cortices were dissected under a stereotactic microscope and homogenized with a potter in Dounce Buffer (HBSS containing 15 mM HEPES buffer and 0.54% glucose). The cell suspension was passed through a pre-wet (with HBSS) 70 μm cell strainer and spun down at 300

g for 10 min at 4°C. Cell pellets were resuspended in 30% Percoll (GE Healthcare) in HBSS and spun for 25 min at 1200g at 4°C. The top myelin layer was discarded and pelleted cells were washed once with HBSS, centrifuged for 5 min at 300g and resuspended in 50 µl of FACS buffer (2% FBS, 1 mM EDTA, 1 × PBS; sterile filtered). For flow cytometry analyses, single cell suspensions underwent live/dead staining (Zombie Aqua, Biolegend) at 1:1000 dilution in PBS for 20 min at 4°C. Fc-receptor blockade was performed using CD16/32 blocking antibody (1:200; BioLegend, cat. no. 553141) incubated 10 min on ice. Surface staining was performed for 30 min on ice with the following antibodies: CD11b (M1/70, BioLegend, 101216), CD45 (30-F11, Biolegend, 103129), Ly6C (HK1.4, Biolegend, 128025), Ly6G (1A8, Biolegend, 127653), and CD121a (IL-1 R, Type I/p80) (JAMA-147, Biolegend, 113505). Flow cytometry analysis was performed on Symphony A3 (BD Bioscience). Raw data were analyzed with FlowJo v10.

2.12. Western blotting

Hippocampi and cortices from WT and *Il1r1*$^{-/-}$ were dissected and homogenized in 62.5 mM Tris pH 8, 290 mM sucrose, 1% sodium dodecyl sulfate (SDS) supplemented with protease inhibitors (Roche) or RIPA buffer (10 mM Tris-HCl, pH 7.5, 150 mM NaCl, 2% Nonidet P-40, 5 mM EDTA, 0.1 mM phenylmethylsulfonyl fluoride, 1 mM β-glycerophosphate, 1 mM sodium orthovanadate, 10 mM sodium fluoride, 0.1 M SDS, 1% protease inhibitor cocktail-Sigma Aldrich). The total protein concentration of each sample was determined by BCA (Thermo Fisher), and equal amounts of total protein (15 µg) were loaded onto 12% Tris–HCl gels (Bio-Rad). Following electrophoresis, proteins were transferred to a 0.45 µm nitrocellulose membrane (Bio-Rad). Blots were probed overnight at 4°C with primary antibodies (mTOR (1:500); p-mTOR (1:500), anti-puromycin (1:5000); anti CYFIP1 (1:1000) anti- C1q (1:1000)) and next incubated with HRP-conjugated secondary antibodies at 1:5000 for 2 hr at Room Temperature. ECL Prime Western Blotting Detection Reagent (GE Healthcare) was used for the detection of the signal. Visualization and imaging of blots were performed using the ChemiDoc system and analyses were conducted using Image Lab (Bio-Rad) or ImageJ software. For each experiment values were normalized on the internal control.

2.13. Real-Time quantitative PCR (RT-qPCR)

The total RNA was extracted from microglia cell culture. The RNA was extracted according to the procedure previously described (Borreca et al., 2015). 500 µl of Trizol was added to tissue or cells and incubated for 5 min to allow complete dissociation of the nucleoproteins complex. 0.1 mL of chloroform was added to the mixture securely capped the tube, then thoroughly mixed by shaking. The sample was centrifuged for 15 min at 12,000 × g at 4°C and the aqueous upper phase was transferred in a new tube. Then 5–10 µg of RNase-free glycogen as a carrier to the aqueous phase and 0,7 volumes of isopropanol (0,350 mL) were added and allowed to precipitate at −80 °C for 1 h. Samples were then centrifuged for 10 min at 12,000 × g at 4°C and the pellet resuspended in 1 mL of 75% ethanol. Finally, the tubes were centrifuged for 5 min at 7500 × g at 4°C, the supernatant discarded and the pellet resuspended in 20–50 µl of RNase-free water. The eluted RNA was quantified with NANOdrop 2000c spectrophotometer (Thermo Fisher Scientific) for RNA concentration and 260/280 nm optical density ratios. 500 ng RNA for each condition underwent reverse transcription into cDNA with High- Capacity cDNA RT kit (Applied Biosystems). Quantitative Real-time polymerase chain reaction (qRT-PCR) was performed with TaqMan detection kit (TaqMan Fast Universal PCR Master Mix(2x), no AmpErase UNG, ThermoFisher) into qRT-PCR Viia7 software system (Applied Biosystems) in a final volume of 10 µl. Each gene was subjected to at least duplicate measurements and data analyses were performed with the comparative Δ*Ct* method. mRNA measurements for target gene were normalized to the housekeeping gene *Gapdh*. The following TaqMan assay was used (Applied Biosystems): mouse *Il1r1* FAM-MGB Mm00434237_m1.

2.14. ELISA immunoassay

For ELISA assay from brain tissue, hippocampi were solubilized in lysis buffer (Tris–HCl 50 mM, Triton X-100 0.1%, EDTA 2 mM, protease inhibitor cocktail) with Tissue Lyser III (Qiagen, Germany), centrifuged at 1,600 g for 15 min, and then, the supernatant was collected. Briefly, 96-well ELISA plates (Nunc MaxiSorp, Thermo Fischer Scientific, Roskilde, Denmark) were coated with a monoclonal antibody in coating buffer (15 mM carbonate buffer pH 9.6) and incubated overnight at 4°C. After each step, plates were washed three times with washing buffer (PBS containing 1.17 mM $CaCl_2$, 1.05 mM $MgCl_2$ and 0.05% Tween 20, pH 7.00). Non-specific binding sites were blocked with 5% dry milk in the washing buffer. Standard or samples were added in duplicate and incubated for 2 h at 37°C. Then, plates were washed and the biotinylated monoclonal antibody diluted in the washing buffer was added. The plates were kept for 1 h at 37°C, washed, and incubated with streptavidin–horseradish peroxidase (Amersham, Milan, Italy). After 1 h incubation at room temperature, the plates were washed extensively before the addition of 100 µl of tetramethylbenzidine substrate (Thermo Fischer Scientific, Rockford, IL, USA). The reaction was blocked with 2N sulfuric acid. Absorbance was measured at 450 nm with an automatic ELISA reader. The mean of cytokines content was obtained by converting Abs 450 values to protein concentration using the standard curve.

2.15. Behavioral tests

Open field: Mice were left to freely move for 30 min in an open field arena (25 cm long and 25 cm wide) and their behavior was recorded with Activity Monitor Software (Med Associates, Inc.). Time or path in the center or periphery of the arena was measured. Open field test was validated in other ASD mouse models at different developmental stages (Larner et al., 2021; Moy et al., 2008; Filipello et al., 2018).

Marble burying: For the marble burying test mice were left to explore a cage with 12 marbles for 30 min and the number of marbles buried or moved was counted. Marble burying was assessed as previously described (Deacon RMJ, 2005).

Self-grooming: Mice were scored for spontaneous grooming behaviors as described earlier (Silverman et al., 2011) with slight modifications. Each mouse was placed individually into a clean mouse cage with a thin (0.5 cm) layer of bedding reducing neophobia, while preventing digging, a potentially competing behavior. After 5 min of acclimatization, each mouse was scored with a stopwatch for 10 min for cumulative time spent grooming all body regions by an expert observer.

Novel object recognition: Novel object recognition was used for memory tasks. The protocol was performed according to the following procedure. Mice were left to acclimate in the arena for 10 min for two consecutive days. On the third day, mice spent 10 min in the arena with two identical objects (LO and RO). After one hour mice were tested for short memory and one of the two objects was substituted with a new one (Familiar object: FO and novel object: NO). Mice were left to explore the object for 10 min and time spending to sniff the object was measured using ETHOVISION software. For the discrimination index the following formula was used: Time spent to the NO– Time spent to FO/ total time *100.

Sociability: Sociability and social novelty tasks were performed as previously described (Corradini et al., 2014). The apparatus consists of a 3-compartment transparent polycarbonate box (20x40x22(h) cm each), with two sliding doors (5x8(h) cm), opening on the central compartment, that can be closed to confine the animal. The proband mouse was habituated in the central compartment for 5 min. For sociability assessment, an unfamiliar adult C57/BL6 male mouse was placed in one side compartment whereas the opposite contained an empty wire cage and mice were left to explore for 10 min. Immediately after the

sociability task, the social novelty test was carried out in the same apparatus without any cleaning, placing a new unfamiliar mouse in the wire cage that had been empty during the prior 10-minute session. Familiar and unfamiliar animals from different home cages had never been in physical contact with the subject mice or with each other. For both tests, the time spent in each chamber was recorded and the time sniffing the conspecific or empty cage was measured. The discrimination ratio was measured according to the following formula: ((time spent towards conspecific mice - time spent toward the inanimate object)/ total time) *100).

Light/dark chamber: The test was performed according to previous studies (Bourin & Hascoët, 2003). The apparatus consisted of a cage divided into a dark compartment (one third) and a brightly illuminated compartment (two thirds). Mice were allowed to freely move for 10 min between the two chambers. The total number of transitions, the time spent in each chamber, the latency to enter the dark chamber and the latency to the first exit from the dark chamber were recorded. After each trial, all chambers were cleaned with ethanol to prevent a bias based on olfactory cues.

Elevated plus maze: The test was performed according to previous studies (Walf & Frye, 2007). The apparatus consisted of a four arms maze with two of them open. Mice were placed on the junction of four arms, facing an open arm and the following parameters were recorded: number of entries in open arms/total entries and time spent in open arms/total. For the number of entries, we considered when animals entry totally the arm.

2.16. Golgi staining

WT or *Il1r1*$^{-/-}$ mice were deeply anesthetized with ketamine (100 mg/kg)/xylazine (20 mg/kg) and perfused transcardially with 0.9% saline solution ($N = 7$ mice per group). Brains were dissected and immediately immersed in a Golgi-Cox solution (1% potassium dichromate, 1% mercuric chloride, and 0.8% potassium chromate) at room temperature for 6 days according to a previously described protocol (Gibb & Kolb, 1998). On the seventh day, brains were transferred to a 30% sucrose solution for cryoprotection and then sectioned with a vibratome. Coronal sections (100 μm) were collected and stained according to the method described by Gibb and Kolb (1998). Sections were stained through consecutive steps in water (1 min), ammonium hydroxide (30 min), water (1 min), developer solution (Kodak fix 100%, 30 min), and water (1 min). Sections were then dehydrated through successive steps in alcohol at rising concentrations (50%, 75%, 95%, and 100%) before being closed with slide cover slips. Spine density was analyzed on CA1 neurons. Neurons were identified with a light microscope (DMI8) under low magnification (20X/NA 0.5) and the 63X immersed oil objective was used for quantification. Five neurons within each hemisphere were taken from each animal. On each neuron, five 30–100 μm dendritic segments of secondary and tertiary branch order of CA1 dendrites were randomly selected and counted using ImageJ software. Only protrusions with a clear connection of the head of the spine to the shaft of the dendrite were counted as spines. Statistical comparisons were made on single neuron values obtained by averaging the number of spines counted on segments of the same neuron. The Data analysis was blinded to the operator.

2.17. Quantification and statistical analysis

Data are displayed as individual dots and mean ± SEM. For each graph, the number of observations indicated with "n'' and the number of biological replicates (mice) indicated with "N'' can be found in the figure legends. Differences between multiple groups were analyzed by One-Way Anova and Two-Way Anova with Bonferroni's or Tukey's post hoc test. Comparisons between two groups following a normal distribution were analyzed using an unpaired *t* test (two-tail distribution), Welch's *t* test or a Mann-Whitney test for two groups with non-normal distribution, as indicated in each figure. Statistical analysis was performed using GraphPad Prism (Graph-Pad Software). Differences were considered to be significant for $p \leq 0.05$ (*),$p \leq 0.01$ (**), $p \leq 0.001$ (***) or $p \leq 0.0001$ (****).

3. Results

3.1. Juvenile *Il1r1*$^{-/-}$ mice display ASD-like behavioral defects and excessive glutamatergic synapses at early developmental stages

We first investigated whether mice lacking IL1 signaling (*Il1r1*$^{-/-}$) display behavioral alterations at early stages of development (P20). Using the open field task, we observed that both WT and *Il1r1*$^{-/-}$ genotypes spent a significantly higher amount of time in the peripheral zones, in the absence of differences between genotypes (Fig. 1A). When checked for the general locomotor activity, *Il1r1*$^{-/-}$ and WT mice displayed a comparable distance traveled, ambulatory counts and resting time (Supplementary Fig. 1A–C). The analysis of stereotyped behaviors revealed significantly enhanced marble burying in *Il1r1*$^{-/-}$ mice relative to WT (Fig. 1B) which, at early postnatal stages, bury a very limited number of marbles (Menashe et al., 2022). Also, *Il1r1*$^{-/-}$mice displayed enhanced self-grooming activity relative to WT (Fig. 1C). When examined in the light/dark chamber, P20 *Il1r1*$^{-/-}$ mice did not display any significant phenotype compared to WT, with no differences detected in any parameter analyzed (Fig. 1D). Furthermore, mice lacking IL-1 signaling displayed sociability deficits, spending significantly less time, compared to WT, in the chamber containing a conspecific mouse relative to an inanimate object (Fig. 1E). In addition, the novel object recognition (NOR) test, which assesses hippocampal-dependent behavior, demonstrated that juvenile *Il1r1*$^{-/-}$ mice display significant defects in spatial learning compared to WT mice (Fig. 1F), not due to an intrinsic preference of animals towards a side of the cage (Supplementary Fig. 1D). These data indicate that juvenile *Il1r1*$^{-/-}$ mice exhibit typical behavioral deficits observed in established mouse models of ASD (Borreca et al., 2023; Gonatopoulos-Pournatzis et al., 2020; Zhou et al., 2016), and in ASD patients (Wang et al., 2023; James et al., 2022; Banker et al., 2021). At P90, both WT and *Il1r1*$^{-/-}$ mice were found to spend comparable time in the center and periphery of the arena (Supplementary Fig. 1E), with genetically mutated mice traveling a significantly higher distance compared to WT (Supplementary Fig. 1F), as previously described (Murray et al., 2013). Differently from juvenile mice, in the light/dark chamber, P90 *Il1r1*$^{-/-}$ mice spent less time in the dark area (Supplementary Fig. 1G) and exhibited a significantly increased number of transitions (Supplementary Fig. 1H); consistently, *Il1r1*$^{-/-}$ mice spent increased time in the open arm in the elevated plus maze (Supplementary Fig. 1I), in line with the anxiolytic-like behavior previously described (Koo & Duman, 2009). Interestingly, *Il1r1*$^{-/-}$ P90 mice maintained defective sociability (Supplementary Fig. 1J), excessive self-grooming (Supplementary Fig. 1K), enhanced marble burying (Supplementary Fig. 1L), and defective NOR (Supplementary Fig. 1M), suggesting the persistence of the autistic-like phenotype even in the adult.

Given the hippocampal contribution to social and cognitive defects in ASD (Banker et al., 2021) and the centrality of synaptic connectivity in the regulation of behavioral phenotypes, the number of hippocampal glutamatergic synapses was evaluated in *Il1r1*$^{-/-}$ P20 mice. We found that the density of synaptic puncta, identified by either presynaptic (vGLut1) or postsynaptic (PSD95) markers in the CA1 hippocampal region (Fig. 2A) was significantly higher in juvenile *Il1r1*$^{-/-}$ mice compared to WT (Fig. 2B–C). Accordingly, Golgi staining demonstrated a higher synaptic spine density (Fig. 2D), in both the apical (Fig. 2E) and basal (Fig. 2F) dendrites. The higher density of synaptic inputs was mirrored by the functional enhancement of glutamatergic synaptic basal transmission, as described in different experimental contexts (Filipello et al., 2018, see also Yi et al., 2016; Sala et al., 2001; Saglietti et al., 2007; Sando & Südhof, 2021). Indeed, whole-cell patch clamp recordings of

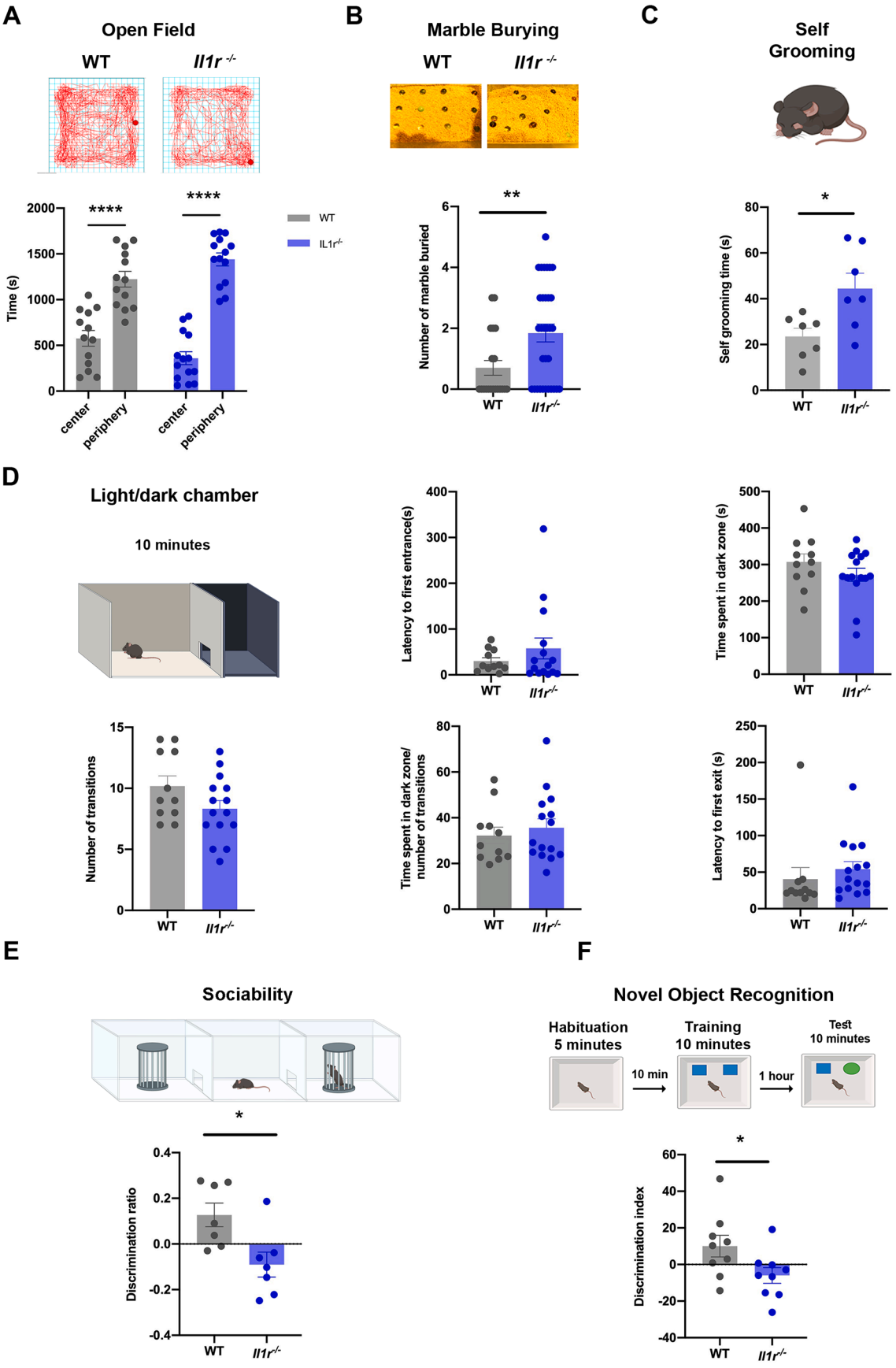

(caption on next page)

Fig. 1. *Juvenile Il1r1*$^{-/-}$ mice display ASD-like behavioral defects. A) Open field test performed at P20: time spent in the center and periphery during a 30 min of arena exploration. Tracks recorded during the open-field session. Both genotypes spent more time in periphery vs center zone of the arena. Two Way Anova followed by Tukey's test for multiple comparison: no significant effect between genotypes $F_{(1,50)} = 3.304e\text{-}30$; $p > 0{,}99$; significant effect between zones $F_{(1,59)} = 122.0$; $p < 0.0001$; significant effect in interaction genotype x zone $F_{(1,50)} = 7.666$; $p = 0.0079$. Post Hoc analysis with Tukey's multiple comparison center vs periphery for both genotypes $p < 0{,}0001$. WT = 13 animals, *Il1r1*$^{-/-}$=14 animals. B) Marble burying test performed at P20: the number of marbles buried in 30 min was evaluated. A significant increase in the number of buried marbles in *Il1r1*$^{-/-}$ compared to WT was observed. Unpaired *t* test with Welch's correction $p = 0{,}0040$. $F_{(31,19)} = 2.325$. WT = 20 animals; *Il1r1*$^{-/-}$=32 animals. C) Self-grooming test performed at P20: *Il1r1*$^{-/-}$ spent more time performing grooming during 10 min recording. Unpaired *t* test $p = 0.0180$. $F_{(6,6)} = 3.411$. WT = 7 animals; *Il1r1*$^{-/-}$=7 animals. D) Light/dark chamber performed at P20: the latency to first entrance in the dark area (unpaired *t* test with Welch's correction $p = 0.2675$; $F_{(14,10)} = 13.13$), the time spent in the dark zone (unpaired *t* test with Welch's correction $p = 0.2337$; $F_{(10,14)} = 1.123$), the number of transitions (unpaired *t* test $p = 0.0956$; $F_{(10,14)} = 1.140$), ratio time spent in the dark/number of transition (unpaired *t* test $p = 0.5425$; $F_{(14,10)} = 1.547$) and the latency to first exit (unpaired *t* test with Welch's correction $p = 0.4735$; $F_{(10,14)} = 1.732$) were evaluated. No differences were observed in *Il1r1*$^{-/-}$ animals compared to WT controls. WT = 11 animals; *Il1r1*$^{-/-}$=15 animals. E) Sociability test performed at P20: during a 10 min test, *Il1r1*$^{-/-}$spent significantly less time exploring a conspecific mouse. The discrimination ratio was evaluated as (time exploring conspecific – time exploring inanimate object)/total time of exploration. Unpaired *t* test $p = 0.0136$; $F_{(6,6)} = 1.121$. WT = 7 animals; *Il1r1*$^{-/-}$=7 animals. F) Novel object recognition task was performed at P20 with animals left to explore two different objects after 1 h of training (with animals exploring two identical objects). A discrimination index was evaluated as (seconds spent toward novel object – seconds spent toward familiar object)/total seconds of exploration*100. Unpaired *t* test $p = 0.0441$. $F_{(8,8)} = 1.914$. WT = 9 animals; *Il1r1*$^{-/-}$=9 animals. The experiments were conducted on different groups of animals, tested in different periods of time.

CA1 pyramidal neurons in acute brain hippocampal slices (Fig. 2G) showed a higher frequency (Fig. 2H) and amplitude (Fig. 2I) of miniature excitatory potential synaptic currents (mEPSCs) in *Il1r1*$^{-/-}$ relative to WT mice. Interestingly, synaptic basal transmission recorded in mixed cultures of neurons and astrocytes, established from embryonic WT and *Il1r1*$^{-/-}$ mice (Supplementary Fig. 2A), revealed no changes in mEPSC frequency (Supplementary Fig. 2B) and amplitude (Supplementary Fig. 2C), suggesting that the phenotype observed in *Il1r1*$^{-/-}$ hippocampal slices cannot be ascribed to neuron- or astrocyte-autonomous mechanisms, but it is likely depending on additional cell types.

3.2. Microglia lacking IL-1R1 exhibit impaired synapse engulfment

The lack of an effect of the *Il1r1*$^{-/-}$ genotype in neuronal cultures prompted us to investigate the putative role of microglia cells in the observed phenotype. Microglia-dependent synapse elimination deficits have been associated with an altered number of synaptic contacts and ASD-like behavior (Tang et al., 2014; Filipello et al., 2018). Hence, we first evaluated whether microglia genetically devoid of *Il1r1* display defects in the phagocytosis of synaptic components *in vivo*. Using a combination of different methods, we first checked whether WT microglia endogenously express IL-1R1. The expression of *Il1r1* transcript was evaluated *via* qPCR in mature microglial cultures both in basal condition and upon LPS stimulation. *Il1r1* transcript was clearly detectable under basal conditions, with a mild upregulation of the transcript upon LPS stimulation, as previously described (Lively & Schlichter, 2018) (Fig. 3A). Immunostaining against IL-1R1 in IBA1^{+}microglia in the hippocampus of WT mice at P20 revealed a positive IL-1R1 staining, organized as distinct clusters distributed throughout microglia cell bodies and processes (Fig. 3B). In line with available RNA-seq databases (https://research-pub.gene.com/BrainMyeloidLandscape/BrainMyeloidLandscape2/#Mouse-gene/Mouse-gene/16177/geneReport.html) (Datasets: GSE52564, (Zhang et al., 2014); Datasets: GSE75246, (Srinivasan et al., 2016)), both *Il1r1* transcript and protein expression in microglia were found to be lower compared to the ones found in astrocytes (Fig. 3A–B). The endogenous protein expression of IL-1R1 was further confirmed by FACS analysis on CD11b^{+}CD45^{int} microglia isolated *ex vivo* from cortices and hippocampi of WT mice at P20 and P90. Both hippocampal and cortical microglia express detectable levels of IL-1R1 protein at P20, which progressively increase at P90 (Fig. 3C–E). Thus, WT microglia express detectable levels of IL-1R1 receptor both *in vitro* and *in vivo* at juvenile (P20) and adult (P90) stages. We then performed a quantitative analysis of synaptic material engulfed inside microglia localized in the hippocampal CA1 region of P20 WT or *Il1r1*$^{-/-}$ mice (Fig. 3F). We found that *Il1r1*$^{-/-}$ microglia exhibited a lower amount of PSD95^{+} material inside CD68^{+} phagolysosome structures (Fig. 3G), without significant changes in CD68 content (Fig. 3H). The reduced phagocytic activity of *Il1r1*$^{-/-}$ microglia was not accompanied by alterations in microglial morphology, as shown by the analysis of the soma size, branching and junctions (Supplementary Fig. 3A–D) in hippocampal microglia from WT or *Il1r1*$^{-/-}$ mice at P20. Moreover, immunostaining for IBA1 at different postnatal stages revealed no change of microglia cell density along the development, except for a slight and transient increase at P9 (Supplementary Fig. 3E). The reduced synapse engulfment did not depend on the lower expression of molecules crucially involved in the regulation of microglia-dependent synaptic pruning. No reduction of the microglial immune receptor TREM2 was detected in microglia from *Il1r1*$^{-/-}$ mice (Supplementary Fig. 3F–G). Also, the C1q complement component, the "eat-me" signal for synapses that need to be eliminated (Stevens et al., 2007), was not reduced but rather increased in synaptosomes isolated from *Il1r1*$^{-/-}$ mice (Supplementary Fig. 3H–I).

To directly assess whether the alteration of the IL-1 pathway in microglia prevents their ability to perform synapse elimination, WT or *Il1r1*$^{-/-}$ microglial cells were co-cultured with WT hippocampal neurons (Fig. 3I). Neurons maintained in contact with WT microglia for 24 h displayed a reduced number of total spines, with lower mushroom and filopodia-like spines density (Fig. 3J–L), consistent with the ability of microglia to phagocytose synapses *in vitro* (Filipello et al., 2018). Conversely, *Il1r1*$^{-/-}$ microglia showed a significantly reduced ability to perform spine elimination compared to WT microglia as indicated by the quantitation of total (Fig. 3J) and mushroom (Fig. 3L) spines. No difference was detected in the density of filopodia in neurons cultured with either WT or *Il1r1*$^{-/-}$ microglia (Fig. 3K), indicating a selective impairment of *Il1r1*$^{-/-}$ microglial cells in pruning mature spine structures. To note, no changes were observed in the release of either pro-inflammatory or anti-inflammatory cytokines by primary WT or *Il1r1*$^{-/-}$ microglia, which could differently guide the microglial synaptic engulfment performance (Supplementary Fig. 3J).

To univocally confirm the inability of *Il1r1*$^{-/-}$ microglia to perform proper synapse phagocytosis, primary WT or *Il1r1*$^{-/-}$ microglia were incubated with synaptosomes prepared from either WT or mutant mice and labeled with FM1-43 fluorescent dye (Fig. 3M, Filipello et al., 2018). Different genetic combinations of microglia and synaptosomes were tested for phagocytic activity. The results indicated that while WT microglia were equally able to engulf synaptosomes from either WT or *Il1r1*$^{-/-}$ mice, *Il1r1*$^{-/-}$ microglia were defective in phagocytosing synaptosomes prepared from either genotype (Fig. 3N). Altogether these data indicate that the lack of IL-1R1 impairs microglia's ability to properly phagocyte synaptic structures during neuronal development.

3.3. Defective phagocytosis is governed by enhancement of mTOR signaling in *Il1r1*$^{-/-}$ microglia

We next aimed to define the molecular pathways responsible for the defective synaptic engulfment in *Il1r1*$^{-/-}$ microglia. It has been reported

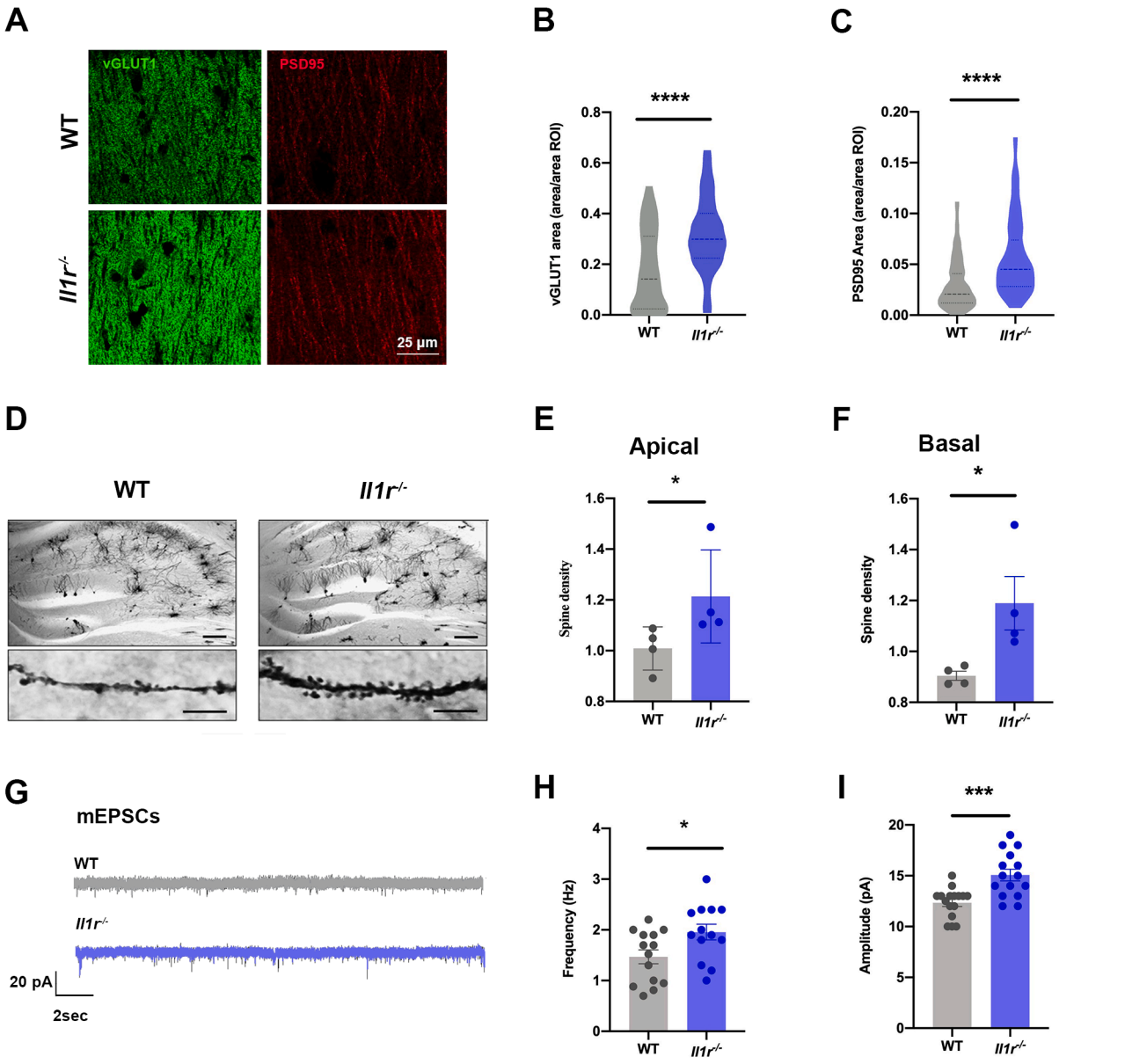

Fig. 2. IL-1R1 Deficient Mice Display altered synaptic density. A) Representative images of pre (vGLUT1) and post (PSD95) synaptic markers in the CA1 hippocampal region of P20 of *Il1r1*$^{-/-}$ and WT mice. Scale bar = 25 mm. Quantitative analysis of vGLUT1 (B) and PSD95 (C) area reveals higher synaptic density for *Il1r1*$^{-/-}$ mice. For vGLUT1 unpaired *t* test with Welch correction $p < 0{,}0001 F_{(47,55)} = 1.238$. For PSD95 unpaired *t* test with Welch correction $p < 0{,}0001$; $F_{(97,96)} = 2.619$. WT = 3 animals; *Il1r1*$^{-/-}$=3 animals. D) Representative images of Golgi staining in hippocampi of P20 WT and *Il1r1*$^{-/-}$ mice. Higher magnifications of dendritic segments are also shown. Quantitative analysis of apical (E) and basal (F) dendrites in CA1 region reveals higher spine density in dendrites of *Il1r1*$^{-/-}$ mice compared to WT. P20 WT N = 4 animals, P20 *Il1r1*$^{-/-}$=4 animals. For each animal a number of 10 dendritic segments were analyzed. For apical dendrites Mann-Whitney test $p = 0{,}0286$; $F_{(3,3)} = 4.670$, for basal dendrites Mann-Whitney test $p = 0{,}0286$; $F_{(3,3)} = 34.20$. Dots represent the mean of 30 segments for each animal, N indicates the number of animals G) Representative traces of mEPSC recordings in CA1 hippocampal acute slices from *Il1r1*$^{-/-}$ and WT mice. Quantitative analysis shows significantly higher mEPSC frequency (H) and amplitude (I). mEPSC frequency: WT 1.468 ± 0.138, n = 14 cells; *Il1r1*$^{-/-}$ 1.956 ± 0.155, n = 13 cells. mEPSC amplitude: WT 12.343 ± 0,361, n = 16 cells; *Il1r1*$^{-/-}$ 15,066 ± 0,554, n = 15 cells. For frequency unpaired *t* test $p = 0{,}0271$; $F_{(12,13)} = 1.185$. For amplitude unpaired *t* test $p = 0{,}003$; $F_{(14,15)} = 2.355$. Scale bars, 20 pA, 2 s. n indicates the number of cells.

that IL-1β enhances the Akt/mTOR metabolic signaling pathway in CD4^{+} T cells (Wyszynski et al., 2016). Unexpectedly, primary microglia isolated from *Il1r1*$^{-/-}$ mice, displayed enhanced levels of both p-mTOR and mTOR (Fig. 4A). Conversely, no difference in p-mTOR and mTOR was detected in *Il1r1*$^{-/-}$ primary neurons (Fig. 4B).

The mammalian target of rapamycin (mTOR) exists in two complexes, mTORC1 and mTORC2. mTORC1 is activated by AKT signaling and leads to autophagy inhibition and increased protein synthesis. In line with excessive mTOR activation in *Il1r1*$^{-/-}$ microglia, SunSET assay revealed elevated protein synthesis in *Il1r1*$^{-/-}$ microglia cells (Supplementary Fig. 4A–B). The elevated protein synthesis activity was also confirmed by the reduction of CYFIP1 protein (Supplementary Fig. 4C–D), a 4EBP binding protein able to negatively regulate eIF4e activation (De Rubeis et al., 2013). Consistently, lower levels of the autophagy-related protein LC3 were found in *Il1r1*$^{-/-}$ microglia compared to WT (Fig. 4C).

To next assess whether the enhancement of mTOR signaling in *Il1r1*$^{-/-}$ microglia could be *per se* responsible for the defects in synapse phagocytosis, we pharmacologically inhibited mTOR activity using rapamycin, a selective mTORC1 inhibitor targeting the subsequent activation of p70-S6 kinase (Ballou & Lin, 2008). The treatment, effective in rescuing mTOR signaling in *Il1r1*$^{-/-}$ microglia (Fig. 4D), was able

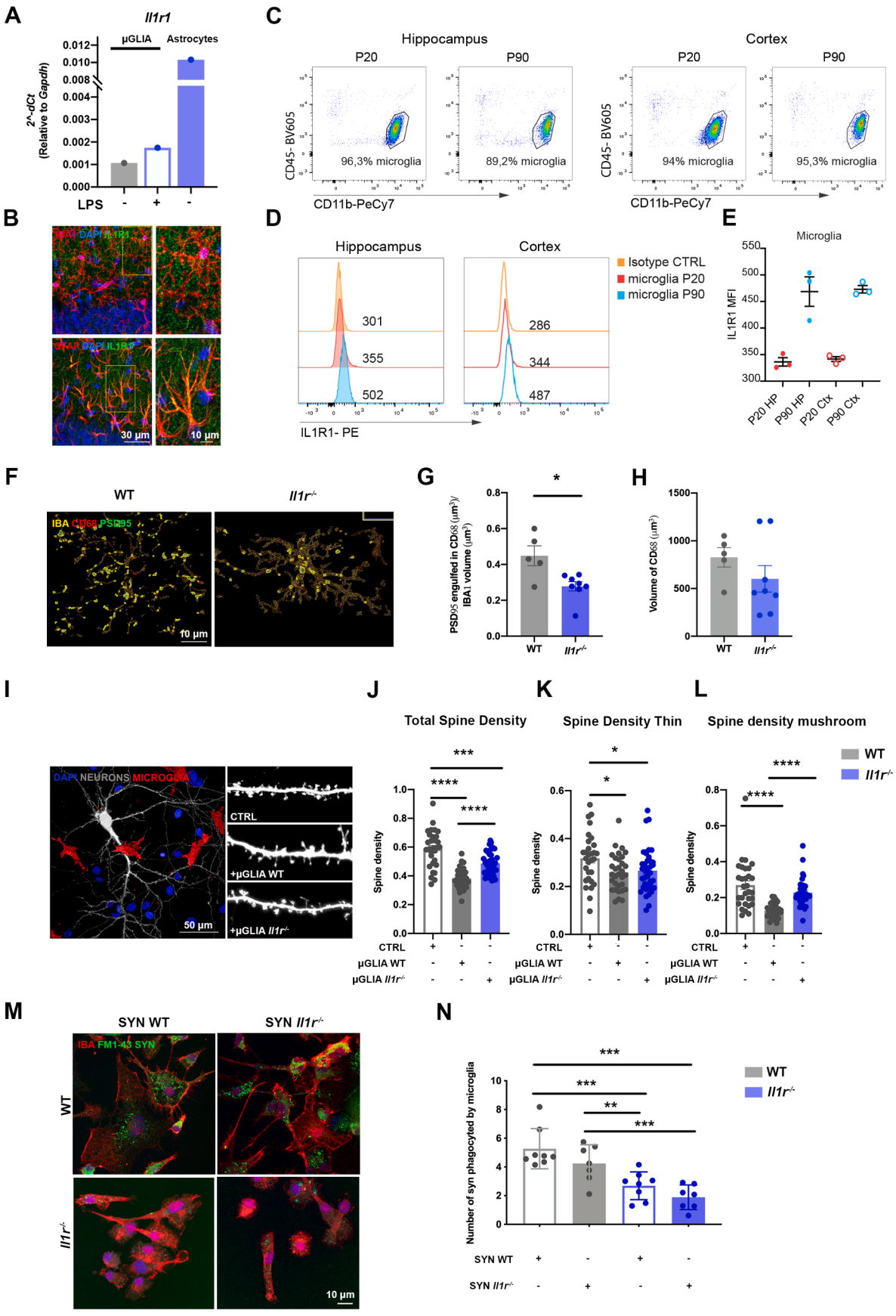

(caption on next page)

Fig. 3. Primary Microglia cells lacking IL-1R1 are Impaired in Synapse Engulfment. A) Real time quantitative PCR performed on primary murine microglia from WT P1-3 pups. Level of *Il1r1* was evaluated in untreated or LPS-treated microglia and in astrocytes. B) Representative immunofluorescence images depicting IL-1R1 expression in Iba1^{+} and Gfap^{+} cells. Scale bar = 30 μm; 10 μm. C) Dot plots of microglia (CD11b^{+}CD45^{int}Ly6C^{-}Ly6G^{-}) isolated from hippocampi and cortices of WT mice. D) Distribution of Mean fluorescence intensity (MFI) values of surface IL-1R1 in microglia from P20 and P90 mice and E) relative quantification. F) Representative images of P20 *Il1r1*$^{-/-}$ and WT P20 hippocampal CA1 region stained by immunofluorescence for IBA1 (microglia marker), CD68 (phagolysosomal marker) and PSD95 (post-synaptic marker). Scale bar = 10 μm. G) Quantitative analysis of PSD95 engulfed in CD68-positive organelles in IBA1^{+} cells. Unpaired *t* test with Welch's correction p = 0,0331, $F_{(4,7)} = 2.902$H) Quantitation of CD68 volume. Unpaired *t* test with Welch's correction p = 0,2160; $F_{(4,7)} = 2.992$. P20 WT = 5 animals; P20 *Il1r1*$^{-/-}$=8 animals. I) Representative images of primary neuronal and microglia co-cultures. WT neurons were co-cultured with microglia derived from WT or *Il1r1*$^{-/-}$ mice (microglia were prepared from P1-3 mice and cultured for 20 days). Single dendritic segments of hippocampal neurons cultured alone, with WT or *Il1r1*$^{-/-}$ microglia are shown. Quantitation of Total spine density (J), thin (K) and mushroom (L) spine density under the aforementioned conditions. Unpaired *t* test with Welch's correction: Total spine density = neurons CTRL vs neurons with microglia WT p < 0.0001; neurons CTRL vs neurons with microglia *Il1r1*$^{-/-}$ p = 0.12; neurons with microglia WT vs neurons with microglia *Il1r1*$^{-/-}$ p < 0.0001; $F_{(2,99)} = 37.51$. Spine density thin = neurons CTRL vs neurons with microglia WT p = 0.0151; neurons CTRL vs neurons with microglia *Il1r1*$^{-/-}$ p = 0.0354; neurons with microglia WT vs neurons with microglia Il1r1$^{-/-}$ p = 0.7092; $F_{(2,99)} = 3.895$. Spine density mushroom neurons CTRL vs neurons with microglia WT p < 0.0001; neurons CTRL vs neurons with microglia *Il1r1*$^{-/-}$ p = 0.12; neurons with microglia WT vs neurons with microglia *Il1r1*$^{-/-}$ p < 0.0001; $F_{(2,99)} = 22.03$. Dots represent the number of segment analyzed from N = 3 independent experiments M) Representative images of *in vitro* WT and *Il1r1*$^{-/-}$ microglia co-cultured for 24 h and exposed to synaptosomes freshly prepared from hippocampi of either WT and *Il1r1*$^{-/-}$ mice and labeled with FM1-43. Scale Bar = 10 μm. N) Analysis of synaptic material engulfed in microglia under different experimental conditions. Two Way Anova: significant effect for genotype ($F_{(1,26)} = 33,86$; p = 0.000001) and treatment ($F_{(1,26)} = 4,67$; p = 0.04) but no significant effect on interaction genotype Vs treatment ($F_{(1, 26)} = 0.070$; p = 0.79). A Post HOC Fisher analysis; microglia WT with syn WT vs microglia WT with syn *Il1r1*$^{-/-}$ p = 0.097; microglia WT with syn WT vs microglia *Il1r1*$^{-/-}$ with syn WT p = 0.000142; microglia WT with syn WT vs microglia *Il1r1*$^{-/-}$ with syn *Il1r1*$^{-/-}$ p = 0.000006; microglia WT with *Il1r1*$^{-/-}$ vs microglia *Il1r1*$^{-/-}$ with syn WT p = 0.015; microglia WT with syn KO vs microglia *Il1r1*$^{-/-}$ with syn *Il1r1*$^{-/-}$ p = 0.000782. Dots represent the number of fields acquired from N = 3 independent experiments.

to restore the ability of *Il1r1*$^{-/-}$ microglia to phagocytose FM1-43 labeled synaptosomes prepared from either WT or *Il1r1*$^{-/-}$ mice (Fig. 4E–F). These data indicate that the genetic lack of IL-1 signaling enhances microglial mTOR activity which in turn leads to an impairment in the microglia's ability to engulf synapses.

3.4. Acute inhibition of IL-1R1 in microglia enhances mTOR signaling and reduces synaptosome phagocytosis

To assess the direct link between IL-1R1-mediated signaling and mTOR activity, and to exclude possible compensatory mechanisms due to the genetic depletion of IL-1R1, we tested whether acute inhibition of IL-1R1 signaling in WT microglia could recapitulate the impaired *Il1r1*$^{-/-}$ microglia phenotype. Primary microglia established from WT brains of P1-3 pups were exposed to the IL-1R1 antagonist (IL-1Ra) (100 ng/μl for 24 h), a pharmacological inhibitor of IL-1R1, followed by quantitation of synapse engulfment and mTOR activity. Like the genetic model, IL-1Ra significantly increased p-mTOR and mTOR in WT microglia, with p-mTOR enhancement being prevented by the concomitant treatment with rapamycin (Fig. 5A–B). Moreover, in line with the results obtained in *Il1r1*$^{-/-}$ mice, the pharmacological blockade of IL-1R1 signaling in WT microglia by IL-1Ra caused a significant reduction in their ability to engulf FM1-43 labeled synaptosomes, which was again rescued by simultaneous treatment with rapamycin (Fig. 5C–D). These data indicate that the acute inhibition of IL-1R1 signaling in WT microglia is sufficient to induce mTOR engagement thus leading to a prominent deregulation of synaptic engulfment activity.

3.5. ASD-like behavioral defects and proper synapse engulfment by microglia are rescued by rapamycin

To next assess the causal link between the excessive mTOR activation and the behavioral defects observed in *Il1r1*$^{-/-}$ mice, rapamycin (10 mg/kg) was intraperitoneally injected (I.P.) for two days *in vivo* (Sato et al., 2023) (Fig. 5E) and mice were then tested for behavioral tasks at the end of the treatment. The results indicated that rapamycin was able to rescue the defects observed in sociability (Fig. 5F) and marble burying (Fig. 5G) but not self-grooming activity (Fig. 5H). Importantly, treatment with rapamycin was also able to restore the proper synaptic engulfment abilities of *Il1r1*$^{-/-}$ microglia *in vivo* (Fig. 5I–J), thus providing a causal link between IL-1R1 signaling and microglial phagocytic abilities.

4. Discussion

Over the last few years, a growing body of evidence indicated that a tightly regulated level of IL-1β is needed to guarantee proper neuronal functioning. Indeed, elevated levels of IL-1β in the hippocampus, resulting from intraperitoneal or intra-cerebroventricular injection of the cytokine (Oitzl et al., 1993; Gibertini et al., 1995; Barrientos et al., 2004) or through IL-1β inducible expression in mice (Hein Am et al., 2010), negatively affect neuronal circuit function impairing behavioral performance. Consistently, excessive IL-1β impairs long-term potentiation (LTP) in several regions of the hippocampus, including hippocampal CA1 (Bellinger et al., 1993; Ross et al., 2003), CA3 (Katsuki et al., 1990), and dentate gyrus (Murray & Lynch, 1998; Kelly et al., 2003). Also, enhancement of IL-1R signaling, like occurring in IL-1R8 deficient mice, negatively affects spine morphology and plasticity (Tomasoni et al., 2017). On the other hand, reduced IL-1β levels also result in cognitive defects. Indeed, IL-1R1 inhibition *via* the IL-1Ra negatively affects cognitive processes including memory consolidation and behavioral tasks (Spulber et al., 2008; Spulber et al., 2009; Spulber et al., 2011) and even the genetic lack of IL-1β receptor induces dysfunctional behavioral paradigms involving spatial memory, contextual fear conditioning and stress responses (Avital et al., 2003; DiSabato et al., 2021; McKim et al., 2018). Hence, both excessive and lower levels of IL-1β result in deleterious effects on behavioral paradigms, suggesting that finely tuned IL-1β levels in the brain are required for proper consolidation of the behavioral settings.

We now demonstrate that the lack of IL-1β signaling at early developmental stages results in derangements of synapse homeostasis and behavioral defects typical of ASD, indicating that a properly tuned homeostatic IL-1β signaling is necessary for proper brain development at early postnatal stages. To note, ASD-like behavior is also maintained in the adult. The cytokine IL-1 may be released by several brain cell types, including microglia (Terada et al., 2010; Burm et al., 2015;Hanamsagar et al., 2011), astrocytes (Davies et al., 1999), platelets (Thornton et al., 2010) and infiltrated immune cells (Pyrillou et al., 2020). Although we cannot exclude that the lack of IL-1R1 may affect different cell types, our study points to a central role of microglia. Using an array of different techniques, we show that microglia established from early postnatal pups express *Il1r1* transcript and that hippocampal or cortical microglia isolated from WT mice express IL-1R1 protein already at P20, as also confirmed by microglial immunostaining for the receptor in P20 brain sections. Also, we found that, when IL-1R1 is lacking, microglia *in vivo* display reduced engulfment of synaptic material. Notably, even acute exposure of WT microglia in culture to the IL-1R1 antagonist IL-1Ra

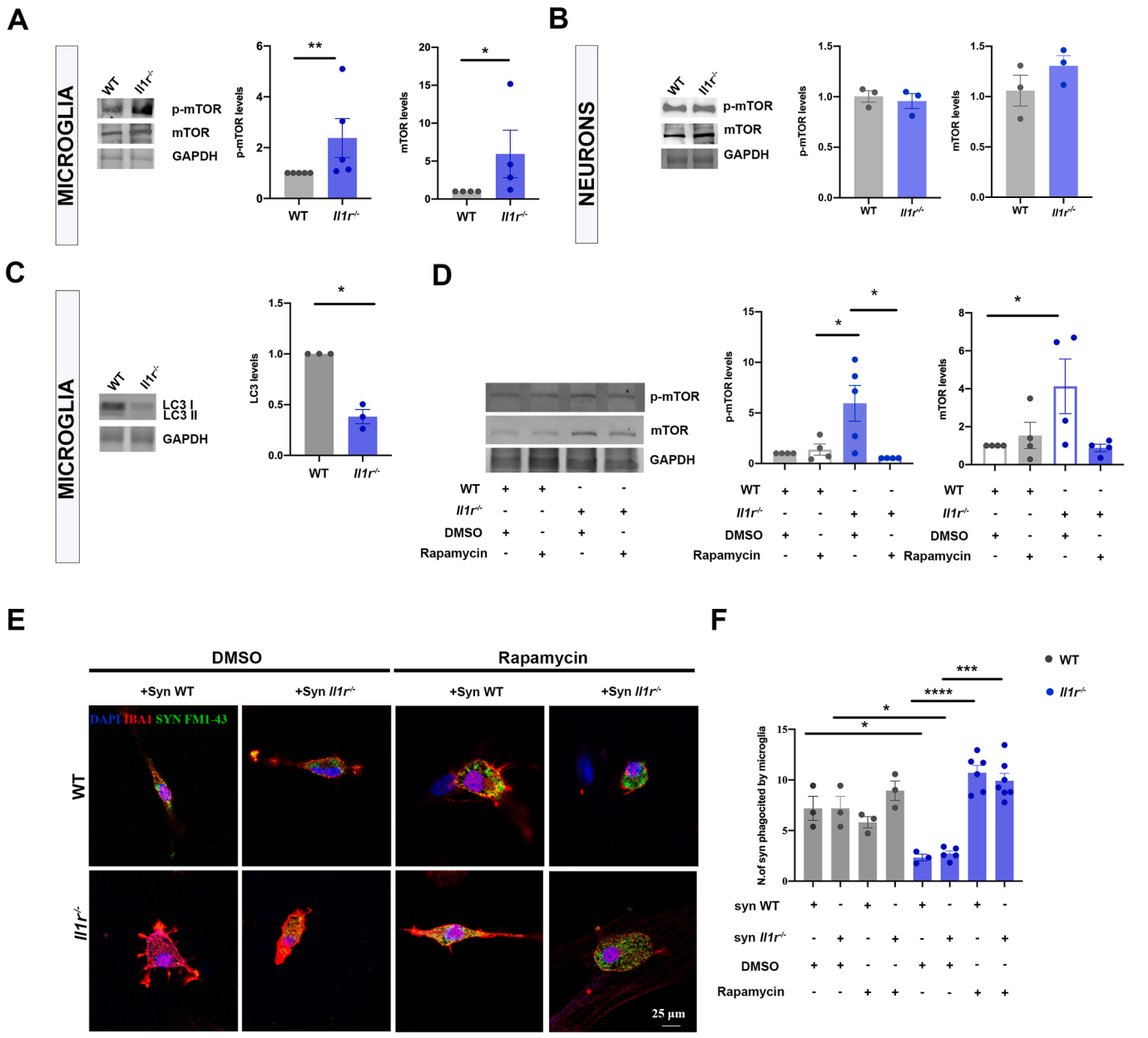

Fig. 4. Enhancement of mTOR in *Il1r1*$^{-/-}$ Microglial Cells is Responsible for Defects in Phagocytic Activity. A) Western Blot images of p-mTOR and mTOR in primary microglia isolated from WT and *Il1r1*$^{-/-}$ mice (microglia were prepared from P1-3 mice and cultured for 20 days) and relative analysis. N = 5 independent experiments. Unpaired *t* test p-mTOR p = 0.007, $F_{(4,4)}$ = infinity; mTOR p = 0.03, $F_{(3,3)}$ = infinity. B) Western Blot images of p-mTOR and mTOR in primary hippocampal neurons isolated from WT and *Il1r1*$^{-/-}$ mice (E17,5) and relative analysis. Unpaired *t* test p-mTOR p = 0.6443, $F_{(2,2)}$ = 1.760; mTOR p = 0.26, $F_{(2,2)}$ = 2.308. WT = 3 different preparations; *Il1r1*$^{-/-}$=3 different preparations. C) Western Blot images of autophagic marker LC3 in primary microglia from WT and *Il1r1*$^{-/-}$ mice (microglia were prepared from P1-3 mice and cultured for 20 days) and relative analysis. Unpaired *t* test p = 0.0125, $F_{(2,2)}$ = infinity. N = 3 independent experiments. D) Western Blot analysis of p-mTOR in microglia treated with rapamycin. No difference was observed in microglia WT not treated (NT) vs microglia WT with DMSO (unpaired *t* test p = 0.5362, F(3,3) = Infinity), while microglia WT DMSO vs microglia *Il1r1*$^{-/-}$ DMSO showed a significant increase of p-mTOR (unpaired *t* test p = 0.0072, $F_{(3,3)}$ = 8.846) which was rescued after rapamycin treatment (microglia *Il1r1*$^{-/-}$ DMSO vs microglia *Il1r1*$^{-/-}$ with rapamycin unpaired *t* test p = 0.0063, $F_{(3,3)}$ = 158102). N = 4 independent experiments. E) Representative images of primary microglia from WT and *Il1r1*$^{-/-}$ mice exposed to synaptosomes from WT and *Il1r1*$^{-/-}$ mice labeled with FM1-43 and F) relative analysis. Two Way Anova (genotype-treatment) was performed followed by Post Hoc Fischer Analysis. A significant interaction genotype x treatment was observed (F(3,25) = 14.60; p < 0.0001) and significant difference between treatment (F(1,25) = 45.03; p < 0.0001). Post Hoc Fischer test reveals a significant difference in: microglia WT with syn WT no treated vs microglia *Il1r1-/-* with syn WT no treated p = 0.0295; microglia WT with syn WT no treated vs microglia *Il1r1*$^{-/-}$ with syn *Il1r1*$^{-/-}$ no treated p = 0.0223; microglia *Il1r1*$^{-/-}$ with syn WT no treated vs microglia *Il1r1*$^{-/-}$ with syn WT treated with rapamycin p < 0.0001, microglia *Il1r1*$^{-/-}$ with syn WT no treated vs microglia WT with syn *Il1r1*$^{-/-}$ treated with rapamycin p = 0.0010; microglia *Il1r1*$^{-/-}$ with syn WT no treated vs microglia *Il1r1*$^{-/-}$ with syn *Il1r1*$^{-/-}$ treated with rapamycin p < 0.0001; microglia *Il1r1*$^{-/-}$ with syn *Il1r1*$^{-/-}$ no treated vs microglia *Il1r1*$^{-/-}$ with syn WT treated with rapamycin p < 0.0001; microglia *Il1r1*$^{-/-}$ with syn *Il1r1*$^{-/-}$ no treated vs microglia WT with syn *Il1r1*$^{-/-}$ treated with rapamycin p = 0.0005; microglia *Il1r1*$^{-/-}$ with syn *Il1r1*$^{-/-}$ no treated vs microglia *Il1r1*$^{-/-}$ with syn *Il1r1*$^{-/-}$ treated with rapamycin p < 0.0001; microglia WT with syn WT treated with rapamycin vs microglia *Il1r1*$^{-/-}$ with syn WT treated with rapamycin p = 0.0065; microglia WT with syn WT treated with rapamycin vs microglia *Il1r1*$^{-/-}$ with syn *Il1r1*$^{-/-}$ treated with rapamycin p = 0.0305. N = 3 independent experiments.

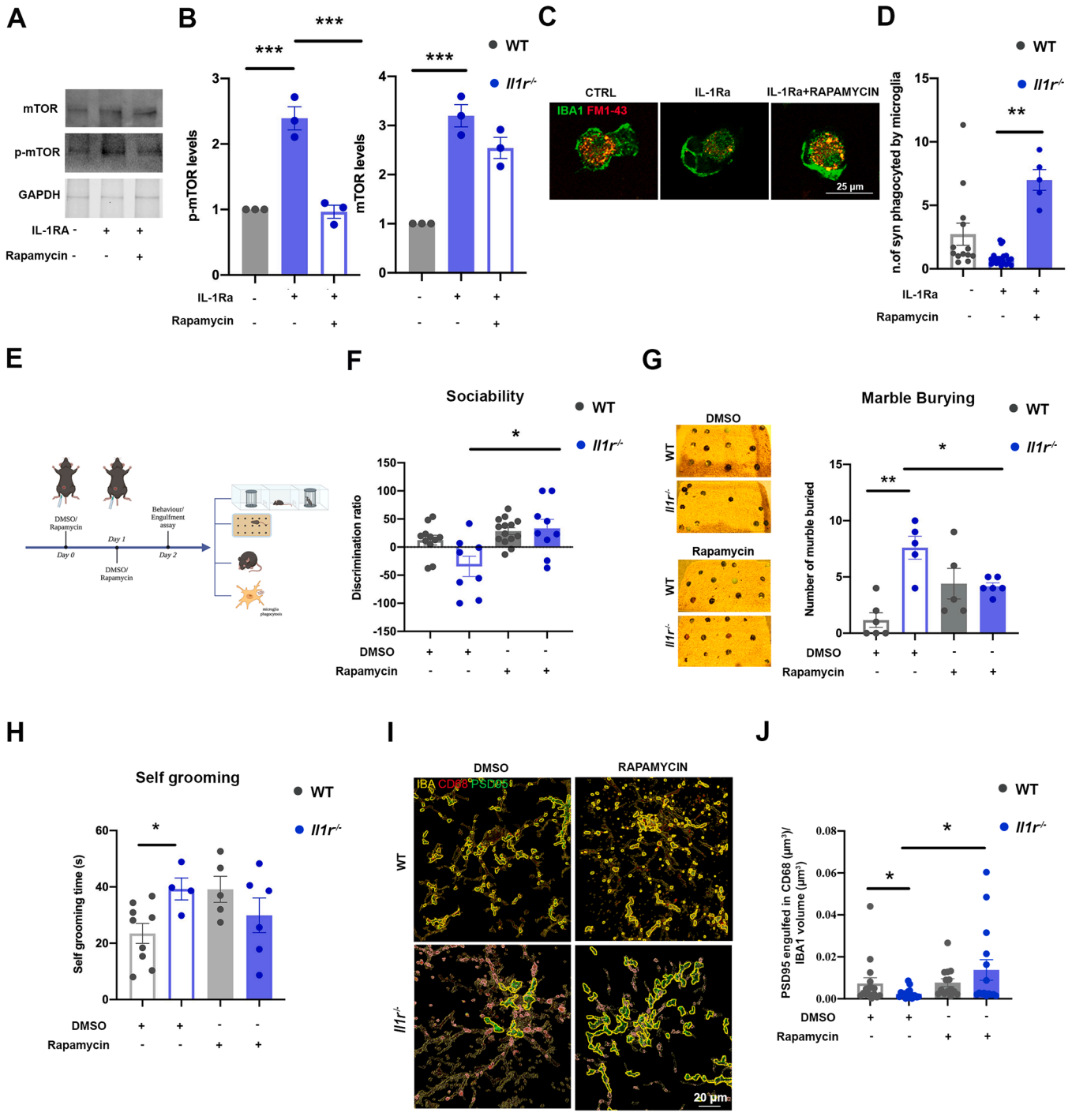

(caption on next page)

Fig. 5. Acute inhibition of IL-1R1 in microglia enhances mTOR signaling and reduces synaptosome phagocytosis. ASD-like behavioral defects and proper synapse engulfment by microglia are rescued by rapamycin. A-B) Western blot Analysis of p-mTOR and mTOR in primary WT microglia treated with IL-1Ra or IL-1Ra + Rapamycin and relative quantitative analysis. p-mTOR unpaired *t* test with Welch's correction: microglia CTRL vs microglia IL-1Ra p = 0.0157, F(2,2) = infinity, microglia IL-1Ra vs microglia IL-1Ra + rapamycin p = 0.0050, $F_{(2,2)} = 3.104$, Ordinary One Way Anova: microglia ctrl vs microglia IL-1Ra p = 0.0004, microglia ctrl vs microglia IL-1Ra + rapamycin p = 0.9771, microglia IL-1Ra vs microglia IL-1Ra + rapamycin p = 0.0003. mTOR unpaired *t* test with Welch's correction: microglia CTRL vs microglia IL-1Ra p = 0.0105, $F_{(2,2)}$ = infinity, microglia IL-1Ra vs microglia IL-1Ra + rapamycin p = 0.1041, $F_{(2,2)} = 1.115$, Ordinary One Way Anova: microglia ctrl vs microglia IL-1Ra p = 0.0003, microglia ctrl vs microglia IL-1Ra + rapamycin p = 0.0023, microglia IL-1Ra vs microglia IL-1Ra + rapamycin p = 0.0934. For analysis N = 3 independent experiments. C) Representative images of WT microglia treated for 24 h with IL-1Ra or IL-1Ra + rapamycin and subsequently exposed to synaptosomes labeled with FM1-43. D) quantitative analysis of synaptosomes engulfed in microglia. Unpaired *t* test microglia IL-1Ra vs microglia IL-1Ra + rapamycin p = 0.0039. N = 3 for each experimental condition. ONE-.WAY Anova P < 0.0001, $F_{(2,35)} = 46.43$. N = 3 for each experimental condition. E) Cartoon depicting the scheme of the experiments. The injection was performed in P20 mice F) Analysis of three-chamber/sociability test in WT and *Il1r1*$^{-/-}$ mice treated or not with rapamycin (injection intraperitoneally of rapamycin for two consecutive days at 5 mg/Kg). Two Way Anova followed by Tukey's analysis for multiple comparison: significant interaction genotype x treatment F(1,38) = 4.928; p = 0.0325. Post Hoc Analysis: *Il1r1*$^{-/-}$ DMSO vs *Il1r1*$^{-/-}$ rapamycin p = 0.0030. WT = 11 animals; *Il1r1*$^{-/-}$=8 animals. WT rapamycin = 14 animals; *Il1r1*$^{-/-}$ rapamycin = 9 animals. G) Analysis of marble burying test in WT and *Il1r1*$^{-/-}$ mice upon rapamycin treatment. Two Way Anova followed by Tukey's analysis for multiple comparison: significant interaction genotype x treatment F(1,17) = 21,47; p = 0.0002. Post Hoc Analysis: *Il1r1*$^{-/-}$ DMSO vs *Il1r1*$^{-/-}$ rapamycin p = 0.0099. WT = 9 animals; *Il1r1*$^{-/-}$=4 animals. WT = 3 animals; *Il1r1*$^{-/-}$=3 animals. WT rapamycin = 5 animals; *Il1r1-/-* rapamycin = 6 animals. H) Analysis of self-grooming in WT and *Il1r1*$^{-/-}$ mice upon rapamycin treatment. Two Way Anova followed by Tukey's analysis for multiple comparison: significant interaction genotype x treatment F(1,20) = 6.46; p = 0.0194. Post Hoc Analysis: *Il1r1*$^{-/-}$ DMSO vs *Il1r1*$^{-/-}$ rapamycin p = 0.74. WT = 3 animals; *Il1r1*$^{-/-}$=3 animals. WT rapamycin = 5 animals; *Il1r1*$^{-/-}$ rapamycin = 6 animals. I) Immunofluorescence staining of hippocampal CA1 region of P20 WT and *Il1r1*$^{-/-}$ mice treated or not with rapamycin for IBA1, CD68 and PSD95. J) analysis of PSD95 engulfed in CD68 in IBA1. Two Way Anova followed by Tukey's analysis for multiple comparison: significant interaction for the treatment F(1,58) = 4.1; p = 0.0474. Post Hoc Analysis: *Il1r1*$^{-/-}$ DMSO vs *Il1r1*$^{-/-}$ rapamycin p = 0.0323. Dots represent the number of fields acquired in N = 3 independent experiments.

results in the reduction of their ability to phagocytose synaptic structures. These data highlight a novel role of IL-1 signaling in the control of microglia-mediated synapse elimination and refinement, strengthening the concept that immune components are key players in the processes of synapse homeostasis in the developing nervous system (Schafer et al., 2012; Matteoli et al., 2023).

Investigation of the molecular mechanisms at the basis of the IL-1-mediated signaling in the process of synapse elimination identified mTOR as a downstream effector of IL-1R1 in microglia. Genetic dysregulation of mTOR signaling is recognized to be at the origin of several neurodevelopmental and neuropsychiatric disorders (Costa-Mattioli & Monteggia, 2013), as occurs for mutations in the ASD-associated genes codifying for the negative regulators of mTORC1, *Tsc1*, *Tsc2* and *Pten* (Sato & Ikeda, 2022; Bahl et al., 2013; Rademacher & Eickholt, 2019). Also, increased p-mTOR levels, accompanied by lower levels of the autophagic marker LC3-II, have been detected in the post-mortem brains of ASD patients (Tang et al., 2014) and in different ASD mouse models (Yan et al., 2018). However, the role of mTOR has been investigated mostly in neurons, where the pathway controls the size of the neuronal soma, axon pathfinding and regeneration (Licausi & Hartman, 2018; Ka et al., 2014; Park et al., 2010), as well as synaptic function and plasticity through the regulation of protein synthesis (Ricciardi et al., 2011; Tsai et al., 2012). Furthermore, a selective enhancement of mTOR in neurons, by suppressing basal neuronal autophagy, was found to cause spine defects and social interaction deficits (Tang et al., 2014). Differently from the above studies, we now provide the evidence that the genetic or pharmacological inactivation of IL-1 signaling at early developmental stages leads to the selective enhancement of the mTOR pathway in microglia, in turn affecting a key biological process that guarantees the proper brain development, i.e. the elimination of supernumerary synapses. Consistently, *Il1r1*$^{-/-}$ mice display increased density of excitatory synaptic contacts (see also Avdic et al., 2015) and dendritic spines. Our data demonstrate that the excessive activation of mTOR in microglia underlies the defective synapse elimination and the ASD-like phenotype. Indeed, treatment of *Il1r1*$^{-/-}$ mice during development with rapamycin is effective in rescuing the correct microglia engulfing activity, both *in vitro* and *in vivo*. Although we cannot exclude the possible contribution of other cell types, the fact that IL-1R1 is expressed in microglia at early developmental stages, together with the observations that mTOR is selectively increased in microglia and that rapamycin rescues microglia synapse engulfment *in vitro* and *in vivo*, eventually rescuing the behavioral defects, indicate that microglia are central to this process. Of note, the mTOR pathway coordinates the mRNA translation machinery resulting in enhanced protein synthesis (), and there is evidence that the upregulation of protein synthesis machinery in microglia induces autistic-like traits (Xu et al., 2020). Whether mTOR signaling in microglia occurs through upstream activators such as PI3K, PD1, AKT which are recruited by IL-1R1 is still to be defined. Our data strengthen the hypothesis that mTOR is a focal point to integrate immune signalling in the brain and that immune dysregulation may converge on mTOR central signaling pathways (Estes & McAllister, 2015).

The enhancement of microglial mTOR activity upon pharmacological inhibition of the IL-1 pathway by the natural IL-1R1 antagonist IL1-Ra, is particularly interesting. IL-1Ra administration has already been shown to impair hippocampal LTP and spatial memory (Yirmiya et al., 2002; Takemiya et al., 2017; Schneider et al., 1998; Goshen et al., 2007). Furthermore, mice genetically overexpressing IL-1Ra display impairments in spatial and contextual memories (Goshen et al., 2007; Spulber et al., 2009). Of note, enhanced circulating levels of IL-1Ra, the natural antagonist preventing IL-1β from binding to its receptor, were detected in ASD children (Saad et al., 2020; Croonenberghs et al., 2002). Whether the IL-1Ra elevation results from an attempt to counterbalance the excessive IL-1β is still undefined (Goines & Ashwood, 2013). The detrimental role of IL-1Ra is also confirmed by the occurrence of polymorphism of the IL-1Ra gene in children with ASD (Saad et al., 2020; Pekkoc Uyanik et al., 2022) as well as by the observation that, when administered during critical windows of neurodevelopment, IL-1Ra can negatively impact neurogenesis, brain morphology, memory consolidation, and behavior (Spulber et al., 2008; Spulber et al., 2009; Spulber et al., 2011).

In conclusion, our results demonstrate that the endogenous IL-1 pathway, a fundamental component of the innate immune response (Dinarello, 1996; Mantovani et al., 2019), has a crucial role in proper brain development and function, and supports the so-called "Goldilocks" state typical of many cytokines (Goines & Ashwood, 2013), where elevated or reduced levels of these immune molecules may affect brain homeostasis. Under this perspective, our data support the concept that alterations in IL-1 systems due to genetic mechanisms or environmental exposures may contribute to ASD-like derangements. Furthermore, we also highlight a key role of IL1 signaling in the ability of microglia to properly eliminate supernumerary synapses. This provides a further, crucial, line of evidence of immune contributions to ASD, where the identification of the central role of the microglial mTOR pathway might open important translational perspectives.

CRediT authorship contribution statement

Antonella Borreca: Data curation, Formal analysis, Methodology,

Supervision, Conceptualization, Validation, Project administration, Writing – original draft, Writing – review & editing. **Cristina Mantovani:** Formal analysis, Methodology. **Genni Desiato:** Data curation, Formal analysis, Supervision, Writing – review & editing. **Irene Corradini:** Formal analysis, Investigation, Supervision, Writing – original draft, Writing – review & editing. **Fabia Filipello:** Formal analysis, Writing – review & editing. **Chiara Elia:** Methodology. **Francesca D'Autilia:** Methodology. **Giulia Santamaria:** Methodology. **Cecilia Garlanda:** Supervision, Visualization. **Raffaella Morini:** Methodology, Writing – original draft, Writing – review & editing. **Davide Pozzi:** Conceptualization, Data curation, Formal analysis, Funding acquisition, Investigation, Methodology, Project administration, Resources, Supervision, Validation, Visualization, Writing – original draft, Writing – review & editing. **Michela Matteoli:** Conceptualization, Data curation, Funding acquisition, Investigation, Project administration, Resources, Supervision, Validation, Visualization, Writing – original draft, Writing – review & editing.

Declaration of competing interest

The authors declare that they have no known competing financial interests or personal relationships that could have appeared to influence the work reported in this paper.

Data availability

Data will be made available on request.

Acknowledgements

This work was supported by PRIN (Ministero dell'Università e della Ricerca, Italy, #2017A9MK4R); Ministry of Health (Italy) (Ministero della Salute RF- 201602361571); ERC AdG MATILDA 101055323, European Research Council (Brussel); EraNET Neuron, European Commission (Brussel) JTC2021— Neurodevelopmental Disorders—InflASD to MM; by Cariplo-Telethon (Italy) (Project: GJC21044A) to DP; by FRAXA FOUNDATION (United States of America) to AB, by Fondazione Cariplo (Italy) (Project: 2018-0364) to FFand by Fondazione Cariplo (Italy) (Project: 2019-1973) to IC. We wish to thank Professor Alberto Mantovani (Humanitas University) for Scientific Discussion. We acknowledge the Reviewers of our manuscript who provided valuable suggestions.

Author contributions

A.B. performed and analyzed experiments *in vivo* and *in vitro* in WT and *Il1r1*$^{-/-}$ genotypes, C.M. performed and analyzed synaptic markers and analysis of cytokines, I.C. performed and analyzed part of behavioral experiments, C.G. provided the mouse model, C.E. performed colony maintenance, genotyping, and sample collection, and G.S. and C. E. performed primary microglia preparation. G.D. performed quantitative real time PCR, *ex vivo* immunofluorescence experiments and IF image preparation. C.M. performed and R.M. *in vivo* electrophysiological recordings and assisted in sample preparation. A.B. performed *ex vivo* immunofluorescence experiments. F.F. performed in in vivo microglia sorting. M.M., and D.P. conceived the study. M.M., A.B, D.P, C.M., G.D., I.C. designed, analyzed, and interpreted the data. M.M, A.B., G.D, I.C. and D.P. wrote the manuscript.

Appendix A. Supplementary data

Supplementary data to this article can be found online at https://doi.org/10.1016/j.bbi.2024.01.221.

References

Arganda-Carreras, I., Fernández-González, R., Muñoz-Barrutia, A., Ortiz-De-Solorzano, C., 2010. 3D reconstruction of histological sections: application to mammary gland tissue. Microsc. Res. Tech. 73 (11), 1019–1029. https://doi.org/10.1002/jemt.20829.

Ashwood, P., Krakowiak, P., Hertz-Picciotto, I., Hansen, R., Pessah, I., Van de Water, J., 2011. Elevated plasma cytokines in autism spectrum disorders provide evidence of immune dysfunction and are associated with impaired behavioral outcome. Brain Behav. Immun. 25 (1), 40–45. https://doi.org/10.1016/j.bbi.2010.08.003.

Atladóttir, H.Ó., Thorsen, P., Østergaard, L., Schendel, D.E., Lemcke, S., Abdallah, M., Parner, E.T., 2010. Maternal infection requiring hospitalization during pregnancy and autism spectrum disorders. J. Autism Dev. Disord. 40 (12), 1423–1430. https://doi.org/10.1007/s10803-010-1006-y.

Avdic, U., Chugh, D., Osman, H., Chapman, K., Jackson, J., Ekdahl, C.T., 2015. Absence of interleukin-1 receptor 1 increases excitatory and inhibitory scaffolding protein expression and microglial activation in the adult mouse hippocampus. Cell. Mol. Immunol. 12 (5), 645–647. https://doi.org/10.1038/cmi.2014.87.

Avital, A., Goshen, I., Kamsler, A., Segal, M., Iverfeldt, K., Richter-Levin, G., Yirmiya, R., 2003. Impaired interleukin-1 signaling is associated with deficits in hippocampal memory processes and neural plasticity. Hippocampus 13 (7), 826–834. https://doi.org/10.1002/hipo.10135.

Bahl, S., Chiang, C., Beauchamp, R.L., Neale, B.M., Daly, M.J., Gusella, J.F., Talkowski, M.E., Ramesh, V., 2013. Lack of association of rare functional variants in TSC1/TSC2 genes with autism spectrum disorder. Molecular Autism 4 (1). https://doi.org/10.1186/2040-2392-4-5.

Ballou, L.M., Lin, R.Z., 2008. Rapamycin and mTOR kinase inhibitors. J. Chem. Biol. 1 (1–4), 27–36. https://doi.org/10.1007/s12154-008-0003-5.

Breder, C.D., Dinarello, C.A., Saper, C.B., 1988. Interleukin-1 Immunoreactive Innervation of the Human Hypothalamus. Science 240 (4850), 321–324. https://doi.org/10.1126/science.3258444.

Banker, S. M., Gu, X., Schiller, D., & Foss-Feig, J. H. (2021). Hippocampal contributions to social and cognitive deficits in autism spectrum disorder. In *Trends in Neurosciences* (Vol. 44, Issue 10, pp. 793–807). Elsevier Ltd. https://doi.org/10.1016/j.tins.2021.08.005.

Barrientos, R.M., Sprunger, D.B., Campeau, S., Watkins, L.R., Rudy, J.W., Maier, S.F., 2004. BDNF mRNA expression in rat hippocampus following contextual learning is blocked by intrahippocampal IL-1β administration. J. Neuroimmunol. 155 (1–2), 119–126. https://doi.org/10.1016/j.jneuroim.2004.06.009.

Basilico, B., Morandell, J., Novarino, G., 2020. Molecular mechanisms for targeted ASD treatments. In: Current Opinion in Genetics and Development, Vol. 65. Elsevier Ltd., pp. 126–137. https://doi.org/10.1016/j.gde.2020.06.004

Bellinger, FP, Madamba, S, Siggins, GR, 1993. Interleukin 1 beta inhibits synaptic strength and long-term potentiation in the rat CA1 hippocampus. Brain Res 628 (1-2), 227–234. https://doi.org/10.1016/0006-8993(93)90959-q.

Bennett, M.L., Bennett, F.C., Liddelow, S.A., Ajami, B., Zamanian, J.L., Fernhoff, N.B., Mulinyawe, S.B., Bohlen, C.J., Adil, A., Tucker, A., Weissman, I.L., Chang, E.F., Li, G., Grant, G.A., Hayden Gephart, M.G., Barres, B.A., 2016. New tools for studying microglia in the mouse and human CNS. PNAS 113 (12), E1738–E1746. https://doi.org/10.1073/pnas.1525528113.

Biesemann, C., Grønborg, M., Luquet, E., Wichert, S.P., Bernard, V., Bungers, S.R., Cooper, B., Varoqueaux, F., Li, L., Byrne, J.A., Urlaub, H., Jahn, O., Brose, N., Herzog, E., 2014. Proteomic screening of glutamatergic mouse brain synaptosomes isolated by fluorescence activated sorting. EMBO J. 33 (2), 157–170. https://doi.org/10.1002/embj.201386120.

Boccazzi, M., Raffaele, S., Zanettin, T., Abbracchio, M.P., Fumagalli, M., 2023. Altered purinergic signaling in neurodevelopmental disorders: focus on P2 receptors. In *Biomolecules* Vol. 13, Issue 5, MDPI. https://doi.org/10.3390/biom13050856.

Borreca, A., Gironi, K., Amadoro, G., Ammassari-Teule, M., 2015. Opposite dysregulation of fragile-X mental retardation protein and heteronuclear ribonucleoprotein C protein associates with enhanced APP translation in alzheimer disease. Mol. Neurobiol. https://doi.org/10.1007/s12035-015-9229-8.

Borreca, A., De Luca, M., Ferrante, A., Boussadia, Z., Pignataro, A., Martire, A., Ammassari-Teule, M., 2023. Fmr1-KO mice failure to detect object novelty associates with a post-test decrease of structural and synaptic plasticity upstream of the hippocampus. Sci. Rep. 13 (1) https://doi.org/10.1038/s41598-023-27991-9.

Bourgeron, T. (2009). A synaptic trek to autism. In *Current Opinion in Neurobiology* (Vol. 19, Issue 2, pp. 231–234). https://doi.org/10.1016/j.conb.2009.06.003.

Bourin, M., & Hascoët, M. (2003). The mouse light/dark box test. In *European Journal of Pharmacology* (Vol. 463, Issues 1–3, pp. 55–65). Elsevier. https://doi.org/10.1016/S0014-2999(03)01274-3.

Bruel, A.L., Vitobello, A., Thiffault, I., Manwaring, L., Willing, M., Agrawal, P.B., Bayat, A., Kitzler, T.M., Brownstein, C.A., Genetti, C.A., Gonzalez-Heydrich, J., Jayakar, P., Zyskind, J.W., Zhu, Z., Vachet, C., Wilson, G.R., Pruniski, B., Goyette, A. M., Duffourd, Y., Faivre, L., 2022. ITSN1: a novel candidate gene involved in autosomal dominant neurodevelopmental disorder spectrum. Eur. J. Hum. Genet. 30 (1), 111–116. https://doi.org/10.1038/s41431-021-00985-9.

Burm, S.M., Zuiderwijk-Sick, E.A., T. Jong, A.E.J., Van, J., Der Putten, C., Veth, J., Kondova, I., Bajramovic, J.J., 2015. Inflammasome-induced IL-1β secretion in microglia is characterized by delayed kinetics and is only partially dependent on inflammatory caspases. J. Neurosci. 35 (2), 678–687. https://doi.org/10.1523/JNEUROSCI.2510-14.2015.

Corradini, I., Donzelli, A., Antonucci, F., Welzl, H., Loos, M., Martucci, R., De Astis, S., Pattini, L., Inverardi, F., Wolfer, D., Caleo, M., Bozzi, Y., Verderio, C., Frassoni, C., Braida, D., Clerici, M., Lipp, H.P., Sala, M., Matteoli, M., 2014. Epileptiform activity

and cognitive deficits in SNAP-25+/- mice are normalized by antiepileptic drugs. Cereb. Cortex 24 (2), 364–376. https://doi.org/10.1093/cercor/bhs316.
Corradini, I., Focchi, E., Rasile, M., Morini, R., Desiato, G., Tomasoni, R., Lizier, M., Ghirardini, E., Fesce, R., Morone, D., Barajon, I., Antonucci, F., Pozzi, D., Matteoli, M., 2018. Maternal immune activation delays excitatory-to-inhibitory gamma-aminobutyric acid switch in offspring. Biol. Psychiatry 83 (8), 680–691. https://doi.org/10.1016/j.biopsych.2017.09.030.
Costa-Mattioli, M., Monteggia, L.M., 2013. mTOR complexes in neurodevelopmental and neuropsychiatric disorders. In Nature Neuroscience (vol. 16 (11), 1537–1543. https://doi.org/10.1038/nn.3546.
Croonenberghs, J., Bosmans, E., Deboutte, D., Kenis, G., Maes, M., 2002. Activation of the inflammatory response system in autism. Neuropsychobiology 45 (1), 1–6. https://doi.org/10.1159/000048665.
Davies, C.A., Loddick, S.A., Toulmond, S., Stroemer, R.P., Hunt, J., Rothwell, N.J., 1999. The progression and topographic distribution of interleukin-l expression after permanent middle cerebral artery occlusion in the rat. in. J. Cereb. Blood Flow Metab. 19.
De Rubeis, S., Pasciuto, E, Li, KW, Fernandez, E, Di Marino, D, Buzzi, A, Ostroff, LE, Klann, E, Zwartkruis, FJ, Komiyama, NH, Grant, SG, Poujol, J, Choquet, D, Achsel, T, Posthuma, D, Smit, AB, Bagni, C., 2013. CYFIP1 coordinates mRNA translation and cytoskeleton remodeling to ensure proper dendritic spine formation. Neuron 79 (6), 1169–1182. https://doi.org/10.1016/j.neuron.2013.06.039.
Deacon, R.M.J., 2005. Marble burying behavior is prevented by anxiolytics as well as by motorstimulants. Pharmacopsychiatry 38 (05). https://doi.org/10.1055/s-2005-918875.
Dinarello, C.A., 1996. Biologic basis for interleukin-l in disease. in. The Journal of The American Society of Hematology 87 (6).
DiSabato, D.J., Nemeth, D.P., Liu, X., Witcher, K.G., O'Neil, S.M., Oliver, B., Bray, C.E., Sheridan, J.F., Godbout, J.P., Quan, N., 2021. Interleukin-1 receptor on hippocampal neurons drives social withdrawal and cognitive deficits after chronic social stress. Mol. Psychiatry 26 (9), 4770–4782. https://doi.org/10.1038/s41380-020-0788-3.
Enstrom, A.M., Onore, C.E., Van de Water, J.A., Ashwood, P., 2010. Differential monocyte responses to TLR ligands in children with autism spectrum disorders. Brain Behav. Immun. 24 (1), 64–71. https://doi.org/10.1016/j.bbi.2009.08.001.
Estes, M. L., & McAllister, A. K. (2015). Immune mediators in the brain and peripheral tissues in autism spectrum disorder. In *Nature Reviews Neuroscience* (Vol. 16, Issue 8, pp. 469–486). Nature Publishing Group. https://doi.org/10.1038/nrn3978.
Filiano, A.J., Xu, Y., Tustison, N.J., Marsh, R.L., Baker, W., Smirnov, I., Overall, C.C., Gadani, S.P., Turner, S.D., Weng, Z., Peerzade, S.N., Chen, H., Lee, K.S., Scott, M.M., Beenhakker, M.P., Litvak, V., Kipnis, J., 2016. Unexpected role of interferon-γ 3 in regulating neuronal connectivity and social behaviour. Nature 535 (7612), 425–429. https://doi.org/10.1038/nature18626.
Filipello, F., Morini, R., Corradini, I., Zerbi, V., Canzi, A., Michalski, B., Erreni, M., Markicevic, M., Starvaggi-Cucuzza, C., Otero, K., Piccio, L., Cignarella, F., Perrucci, F., Tamborini, M., Genua, M., Rajendran, L., Menna, E., Vetrano, S., Fahnestock, M., Matteoli, M., 2018. The microglial innate immune receptor TREM2 Is required for synapse elimination and normal brain connectivity. Immunity 48 (5), 979–991.e8. https://doi.org/10.1016/j.immuni.2018.04.016.
French, R.A., Vanhoy, R.W., Chizzonite, R., Zachary, J.F., Dantzer, R., Parnet, P., Bluthe, R.-M., Kelley, K.W., 1999. Expression and localization of p80 and p68 interleukin-1 receptor proteins in the brain of adult mice. In. J. Neuroimmunol. 93.
Gibb, R., Kolb, B., 1998. A method for vibratome sectioning of Golgi-Cox stained whole rat brain. In. J. Neurosci. Methods 79.
Gibertini, M, Newton, C, Friedman, H, Klein, TW, 1995. Spatial learning impaiment in mice infected with Legionella pneumophila or administered exogenous interleukin-1- beta. Brain Behav Immun 9 (2), 113–128. https://doi.org/10.1006/brbi.1995.1012.
Giulian, D., Young, D.G., Woodward, J., Brown, D.C., Lachmanl, L.B., 1988. Interleukin-1 Is an astroglial growth factor in the developing brain. In. J. Neurosci. 8 (2).
Glaccum, M. B., Charrier, K., Willis, C. R., Maliszewski, C., Livingston, D. J., Peschon, J. J., & Morrissey, P. J. (1997). *Phenotypic and Functional Characterization of Mice That Lack the Type I Receptor for IL-1*. http://journals.aai.org/jimmunol/article-pdf/159/7/3364/1078877/3364.pdf.
Goines, P.E., Ashwood, P., 2013. Cytokine dysregulation in autism spectrum disorders (ASD): possible role of the environment. Neurotoxicol. Teratol. 36, 67–81. https://doi.org/10.1016/j.ntt.2012.07.006.
Gonatopoulos-Pournatzis, T., Niibori, R., Salter, E.W., Weatheritt, R.J., Tsang, B., Farhangmehr, S., Liang, X., Braunschweig, U., Roth, J., Zhang, S., Henderson, T., Sharma, E., Quesnel-Vallières, M., Permanyer, J., Maier, S., Georgiou, J., Irimia, M., Sonenberg, N., Forman-Kay, J.D., Blencowe, B.J., 2020. Autism-Misregulated eIF4G microexons control synaptic translation and higher order cognitive functions. Mol. Cell 77 (6), 1176–1192.e16. https://doi.org/10.1016/j.molcel.2020.01.006.
Goshen, I., Kreisel, T., Ounallah-Saad, H., Renbaum, P., Zalzstein, Y., Ben-Hur, T., Levy-Lahad, E., Yirmiya, R., 2007. A dual role for interleukin-1 in hippocampal-dependent memory processes. Psychoneuroendocrinology 32 (8–10), 1106–1115. https://doi.org/10.1016/j.psyneuen.2007.09.004.
Hall, M. B., Willis, D. E., Rodriguez, E. L., & Schwarz, J. M. (2023). Maternal immune activation as an epidemiological risk factor for neurodevelopmental disorders: Considerations of timing, severity, individual differences, and sex in human and rodent studies. In *Frontiers in Neuroscience* (Vol. 17). Frontiers Media S.A. https://doi.org/10.3389/fnins.2023.1135559.
Hanamsagar, R., Torres, V., Kielian, T., 2011. Inflammasome activation and IL-1β/IL-18 processing are influenced by distinct pathways in microglia. J. Neurochem. 119 (4), 736–748. https://doi.org/10.1111/j.1471-4159.2011.07481.x.
Hein Am, Stasko, MR, Matousek, SB, Scott-McKeanJJ, Maier, SF, Olschowka, Ja, Costa, AC, O'Banion, MK, 2010. Sustained hippocampal IL-1beta overexpression impairs contextual and spatial memory in transgenic mice. Brain Behav Immun 24 (2), 243–253. https://doi.org/10.1016/j.bbi.2009.10.002.
Herz, J., Fu, Z., Kim, K., Dykstra, T., Wall, M., Li, H., Salvador, A.F., Zou, B., Yan, N., Blackburn, S.M., Andrews, P.H., Goldman, D.H., Papadopoulos, Z., Smirnov, I., Xie, X.S., Kipnis, J., 2021. GABAergic neuronal IL-4R mediates T cell effect on memory. Neuron 109 (22), 3609–3618.e9. https://doi.org/10.1016/j.neuron.2021.10.022.
Hewett, S. J., #2, N. A. J., & Claycomb, R. J. (n.d.). *Interleukin-1β in Central Nervous System Injury and Repair*.
Hsiao, E.Y., Patterson, P.H., 2011. Activation of the maternal immune system induces endocrine changes in the placenta via IL-6. Brain Behav. Immun. 25 (4), 604–615. https://doi.org/10.1016/j.bbi.2010.12.017.
Huguet, G., Ey, E., Bourgeron, T., 2013. The genetic landscapes of autism spectrum disorders. In. Annu. Rev. Genomics Hum. Genet. 14, 191–213. https://doi.org/10.1146/annurev-genom-091212-153431.
Hutsler, J.J., Zhang, H., 2010. Increased dendritic spine densities on cortical projection neurons in autism spectrum disorders. Brain Res. 1309, 83–94. https://doi.org/10.1016/j.brainres.2009.09.120.
Huttner, W. B., Schiebler, W., Greengard, P., & De Camilli, P. (n.d.). *Synapsin I (Protein I), a Nerve Terminal-Specific Phosphoprotein. III. Its Association with Synaptic Vesicles Studied in a Highly Purified Synaptic Vesicle Preparation*.
Iwamasa, G.Y., 1997. Behavior Therapy and a Culturally Diverse Society: Forging an Alliance. In *BEHAVIOR THERAPY* 28.
James, P., Schafer, E., Wolfe, J., Matthews, L., Browning, S., Oleson, J., Sorensen, E., Rance, G., Shiels, L., Dunn, A., 2022. Increased rate of listening difficulties in autistic children. J. Commun. Disord. 99 https://doi.org/10.1016/j.jcomdis.2022.106252.
Jyonouchi, H., Sun, S., Le, H., 2001. Proinflammatory and regulatory cytokine production associated with innate and adaptive immune responses in children with autism spectrum disorders and developmental regression q. In. J. Neuroimmunol. 120. www.elsevier.comrlocaterjneuroim.
Ka, M., Condorelli, G., Woodgett, J.R., Kim, W.Y., 2014. mTOR regulates brain morphogenesis by mediating GSK3 signaling. Development (cambridge) 141 (21), 4076–4086. https://doi.org/10.1242/dev.108282.
Katsuki, H., Nakai, S., Hirai, Y., Akaji, K.-I., Kiso, Y., Satoh, M., 1990. Interleukin-lfl inhibits long-term potentiation in the CA3 region of mouse hippocampal slices. In *European Journal of*. Pharmacology.
Kelly, Á., Vereker, E., Nolan, Y., Brady, M., Barry, C., Loscher, C.E., Mills, K.H.G., Lynch, M.A., 2003. Activation of p38 plays a pivotal role in the inhibitory effect of lipopolysaccharide and interleukin-1β on long term potentiation in rat dentate gyrus. J. Biol. Chem. 278 (21), 19453–19462. https://doi.org/10.1074/jbc.M301938200.
Kim, J., Kundu, M., Viollet, B., Guan, K.L., 2011. AMPK and mTOR regulate autophagy through direct phosphorylation of Ulk1. Nat. Cell Biol. 13 (2), 132–141. https://doi.org/10.1038/ncb2152.
Koo, J.W., Duman, R.S., 2009. Interleukin-1 receptor null mutant mice show decreased anxiety-like behavior and enhanced fear memory. Neurosci. Lett. 456 (1), 39–43. https://doi.org/10.1016/j.neulet.2009.03.068.
Larner, O., Roberts, J., Twiss, J., Freeman, L., 2021. A need for consistency in behavioral phenotyping for ASD: analysis of the valproic acid model. Autism Res. Treat. 2021, 1–10. https://doi.org/10.1155/2021/8863256.
Lechan, R. M., Toni, R., Clark, B. D., Cannon, J. G., Shaw, A. R., Dinarello, C. A., & Reichlin, S. (1990). Immunoreactive interleukin-l localization in the rat forebrain. In *Brain Research* (Vol. 514).
Xiao-Jing Li 1, M. Z. X.-H. L. Y.-H. X. H. L. M. Y. (2009). Effects of Tanshinone IIa on cytokines and platelets in immune vasculitis and its mechanism. *Zhongguo Shi Yan Xue Ye Xue Za Zhi*, *17*(1), 188–192.
Licausi, F., & Hartman, N. W. (2018). Role of mTOR complexes in neurogenesis. In *International Journal of Molecular Sciences* (Vol. 19, Issue 5). MDPI AG. https://doi.org/10.3390/ijms19051544.
Lim, E.T., Raychaudhuri, S., Sanders, S.J., Stevens, C., Sabo, A., MacArthur, D.G., Neale, B.M., Kirby, A., Ruderfer, D.M., Fromer, M., Lek, M., Liu, L., Flannick, J., Ripke, S., Nagaswamy, U., Muzny, D., Reid, J.G., Hawes, A., Newsham, I., Daly, M.J., 2013. Rare complete knockouts in humans: population distribution and significant role in autism spectrum disorders. Neuron 77 (2), 235–242. https://doi.org/10.1016/j.neuron.2012.12.029.
Lively, S., Schlichter, L.C., 2018. Microglia responses to pro-inflammatory stimuli (LPS, IFNγ+TNFα) and reprogramming by resolving cytokines (IL-4, IL-10). Front. Cell. Neurosci. 12 https://doi.org/10.3389/fncel.2018.00215.
Loureiro, L.O., Howe, J.L., Reuter, M.S., Iaboni, A., Calli, K., Roshandel, D., Pritišanac, I., Moses, A., Forman-Kay, J.D., Trost, B., Zarrei, M., Rennie, O., Lau, L.Y.S., Marshall, C.R., Srivastava, S., Godlewski, B., Buttermore, E.D., Sahin, M., Hartley, D., Scherer, S.W., 2021. A recurrent SHANK3 frameshift variant in Autism Spectrum Disorder. *Npj*. Genomic Medicine 6 (1). https://doi.org/10.1038/s41525-021-00254-0.
Mantovani, A., Dinarello, C.A., Molgora, M., Garlanda, C., 2019. Interleukin-1 and Related Cytokines in the Regulation of Inflammation and Immunity. In: Immunity, Vol. 50(4. Cell Press, pp. 778–795. https://doi.org/10.1016/j.immuni.2019.03.012.
Masi, A., Breen, E.J., Alvares, G.A., Glozier, N., Hickie, I.B., Hunt, A., Hui, J., Beilby, J., Ravine, D., Wray, J., Whitehouse, A.J.O., Guastella, A.J., 2017. Cytokine levels and associations with symptom severity in male and female children with autism spectrum disorder. Molecular Autism 8 (1). https://doi.org/10.1186/s13229-017-0176-2.
Matteoli, M., Pozzi, D., Fossati, M., Menna, E., 2023. Immune synaptopathies: how maternal immune activation impacts synaptic function during development. EMBO J. 42 (13) https://doi.org/10.15252/embj.2023113796.
McKim, D.B., Weber, M.D., Niraula, A., Sawicki, C.M., Liu, X., Jarrett, B.L., Ramirez-Chan, K., Wang, Y., Roeth, R.M., Sucaldito, A.D., Sobol, C.G., Quan, N., Sheridan, J.

F., Godbout, J.P., 2018. Microglial recruitment of IL-1β-producing monocytes to brain endothelium causes stress-induced anxiety. Mol. Psychiatry 23 (6), 1421–1431. https://doi.org/10.1038/mp.2017.64.
Menashe, N., Salama, Y., Steinauer, M.L., Spaan, J.M., 2022. Do behavioral test scores represent repeatable phenotypes of female mice? J. Pharmacol. Toxicol. Methods 115. https://doi.org/10.1016/j.vascn.2022.107170.
Mirabella, F., Desiato, G., Mancinelli, S., Fossati, G., Rasile, M., Morini, R., Markicevic, M., Grimm, C., Amegandjin, C., Termanini, A., Peano, C., Kunderfranco, P., di Cristo, G., Zerbi, V., Menna, E., Lodato, S., Matteoli, M., Pozzi, D., 2021. Prenatal interleukin 6 elevation increases glutamatergic synapse density and disrupts hippocampal connectivity in offspring. Immunity 54 (11), 2611–2631.e8. https://doi.org/10.1016/j.immuni.2021.10.006.
Moy, S. S., Nadler, J. J., Young, N. B., Perez, A., Holloway, L. P., Barbaro, R. P., Barbaro, J. R., West, L. M., Threadgill, D. W., Lauder, J. M., Magnuson, T. R., Crawley, J. N., Moy, S. S., & Holloway, P. (2008). *Mouse Behavioral Tasks Relevant to Autism: Phenotypes of Ten Inbred Strains*. http://aretha.jax.org/pub-cgi/phenome/mpdcgi.
Murray, C. A., & Lynch, M. A. (1998). *Evidence That Increased Hippocampal Expression of the Cytokine Interleukin-1 Is a Common Trigger for Age-and Stress-Induced Impairments in Long-Term Potentiation*.
Murray, C.L., Obiang, P., Bannerman, D., Cunningham, C., 2013. Endogenous IL-1 in cognitive function and anxiety: A study in IL-1RI-/-mice. PLoS One 8 (10). https://doi.org/10.1371/journal.pone.0078385.
O'Connor, J.J., Coogan, A.N., 1999. Actions of the Pro-Inflammatory Cytokine Il-1[beta] on central synaptic transmission. Exp. Physiol. 84 (4), 601–614. https://doi.org/10.1111/j.1469-445x.1999.01892.x.
O'Roak, B.J., Deriziotis, P., Lee, C., Vives, L., Schwartz, J.J., Girirajan, S., Karakoc, E., MacKenzie, A.P., Ng, S.B., Baker, C., Rieder, M.J., Nickerson, D.A., Bernier, R., Fisher, S.E., Shendure, J., Eichler, E.E., 2011. Exome sequencing in sporadic autism spectrum disorders identifies severe de novo mutations. Nat. Genet. 43 (6), 585–589. https://doi.org/10.1038/ng.835.
Oitzl, M. S., Van Oers, H., Sch6bitz, B., Ron De Kloet, E., & Oitzl, M. S. (1993). Interleukin-lfl, but not interleukin-6, impairs spatial navigation learning. In *Brain Research* (Vol. 613).
Pagani, M., Barsotti, N., Bertero, A., Trakoshis, S., Ulysse, L., Locarno, A., Miseviciute, I., De Felice, A., Canella, C., Supekar, K., Galbusera, A., Menon, V., Tonini, R., Deco, G., Lombardo, M.V., Pasqualetti, M., Gozzi, A., 2021. mTOR-related synaptic pathology causes autism spectrum disorder-associated functional hyperconnectivity. Nature Communications 12 (1). https://doi.org/10.1038/s41467-021-26131-z.
Park, K. K., Liu, K., Hu, Y., Kanter, J. L., & He, Z. (2010). PTEN/mTOR and axon regeneration. In *Experimental Neurology* (Vol. 223, Issue 1, pp. 45–50). https://doi.org/10.1016/j.expneurol.2009.12.032.
Patterson, P. H. (2011). Maternal infection and immune involvement in autism. In *Trends in Molecular Medicine* (Vol. 17, Issue 7, pp. 389–394). https://doi.org/10.1016/j.molmed.2011.03.001.
Pekkoc Uyanik, K.C., Kalayci Yigin, A., Dogangun, B., Seven, M., 2022. Evaluation of IL1B rs1143634 and IL6 rs1800796 Polymorphisms with Autism Spectrum Disorder in the Turkish Children. Immunol. Invest. 51 (4), 766–777. https://doi.org/10.1080/08820139.2020.1870489.
Percie Du Sert, N, Hurst, V, Ahluwalia, A, Alam, S, Avey, MT, Baker, M, Brown, WJ, Clark, A, Cuthill, IC, Dirnagl, U, Emerson, M, Garner, P, Holgate, ST, Howells Dw, Karp, NA, Lazic, SE, Lidster, K, Mac Callum, CJ, Macleod, M, Pearl, EJ, Petersen, OH, Rawle, F, Reynolds, P, Rooney, K, Sena, ES, Silberberg, SD, Steckler, T, Wurbel, H, 2020. The ARRIIVE guideline 2.0: Update guidelines for reporting animal research. Plos Biol 18 (7), e3000410. https://doi.org/10.1371/journal.pbio.3000410.
Piton, A., Michaud, J.L., Peng, H., Aradhya, S., Gauthier, J., Mottron, L., Champagne, N., Lafrenière, R.G., Hamdan, F.F., Joober, R., Fombonne, E., Marineau, C., Cossette, P., Dubé, M.P., Haghighi, P., Drapeau, P., Barker, P.A., Carbonetto, S., Rouleau, G.A., 2008. Mutations in the calcium-related gene IL1RAPL1 are associated with autism. Hum. Mol. Genet. 17 (24), 3965–3974. https://doi.org/10.1093/hmg/ddn300.
K. Pyrillou L.C. Burzynski M.C.H. Clarke Alternative Pathways of IL-1 Activation, and Its Role in Health and Disease Frontiers in Immunology Vol. 11 2020 Frontiers Media S. A 10.3389/fimmu.2020.613170.
Rademacher, S., Eickholt, B.J., 2019. PTEN in autism and neurodevelopmental disorders. Cold Spring Harb. Perspect. Med. 9 (11) https://doi.org/10.1101/cshperspect.a036780.
Ravaccia, D., & Ghafourian, T. (2020). Critical role of the maternal immune system in the pathogenesis of autism spectrum disorder. In *Biomedicines* (Vol. 8, Issue 12, pp. 1–21). MDPI AG. https://doi.org/10.3390/biomedicines8120557.
Ren, J., Lu, X., Hall, G., Privratsky, J.R., Robson, M.J., Blakely, R.D., Crowley, S.D., 2022. IL-1 receptor signaling in podocytes limits susceptibility to glomerular damage. Am. J. Physiol. Ren. Physiol. 322 (2), F164–F174. https://doi.org/10.1152/ajprenal.00353.2021.
Ricciardi, S., Boggio, E.M., Grosso, S., Lonetti, G., Forlani, G., Stefanelli, G., Calcagno, E., Morello, N., Landsberger, N., Biffo, S., Pizzorusso, T., Giustetto, M., Broccoli, V., 2011. Reduced AKT/mTOR signaling and protein synthesis dysregulation in a Rett syndrome animal model. Hum. Mol. Genet. 20 (6), 1182–1196. https://doi.org/10.1093/hmg/ddq563.
Rodriguez-Gomez, D.A., Garcia-Guaqueta, D.P., Charry-Sánchez, J.D., Sarquis-Buitrago, E., Blanco, M., Velez-van-Meerbeke, A., Talero-Gutiérrez, C., 2021. A systematic review of common genetic variation and biological pathways in autism spectrum disorder. BMC Neurosci. 22 (1) https://doi.org/10.1186/s12868-021-00662-z.
Ross, F.M., Allan, S.M., Rothwell, N.J., Verkhratsky, A., 2003. A dual role for interleukin-1 in LTP in mouse hippocampal slices. J. Neuroimmunol. 144 (1–2), 61–67. https://doi.org/10.1016/j.jneuroim.2003.08.030.
Saad, K., Abdallah, A.E.M., Abdel-Rahman, A.A., Al-Atram, A.A., Abdel-Raheem, Y.F., Gad, E.F., Abo-Elela, M.G.M., Elserogy, Y.M., Elhoufey, A., Nigm, D.A., Nagiub Abdelsalam, E.M., Alruwaili, T.A.M., 2020. Polymorphism of interleukin-1β and interleukin-1 receptor antagonist genes in children with autism spectrum disorders. Prog. Neuropsychopharmacol. Biol. Psychiatry 103. https://doi.org/10.1016/j.pnpbp.2020.109999.
Saglietti, L., Dequidt, C., Kamieniarz, K., Rousset, M.C., Valnegri, P., Thoumine, O., Beretta, F., Fagni, L., Choquet, D., Sala, C., Sheng, M., Passafaro, M., 2007. Extracellular Interactions between GluR2 and N-Cadherin in Spine Regulation. Neuron 54 (3), 461–477. https://doi.org/10.1016/j.neuron.2007.04.012.
Sala, C., Pië ch, V., Wilson, N. R., Passafaro, M., Liu, G., & Sheng, M. (2001). For instance, long-term potentiation. In *connections (Calverley and Jones* (Vol. 31). Ehlers.
Sanders, S.J., Murtha, M.T., Gupta, A.R., Murdoch, J.D., Raubeson, M.J., Willsey, A.J., Ercan-Sencicek, A.G., Di Lullo, N.M., Parikshak, N.N., Stein, J.L., Walker, M.F., Ober, G.T., Teran, N.A., Song, Y., El-Fishawy, P., Murtha, R.C., Choi, M., Overton, J. D., Bjornson, R.D., State, M.W., 2012. De novo mutations revealed by whole-exome sequencing are strongly associated with autism. Nature 485 (7397), 237–241. https://doi.org/10.1038/nature10945.
Sandin, S., Lichtenstein, P., Kuja-Halkola, R., Larsson, H., Hultman, C.M., Reichenberg, A., 2014. The familial risk of autism. JAMA 311 (17), 1770–1777. https://doi.org/10.1001/jama.2014.4144.
Sando, R., Südhof, T.C., 2021. Latrophilin gpcr signaling mediates synapse formation. Elife 10. https://doi.org/10.7554/eLife.65717.
Sato, A., Ikeda, K., 2022. Genetic and Environmental Contributions to Autism Spectrum Disorder Through Mechanistic Target of Rapamycin. In: Biological Psychiatry Global Open Science, Vol. 2(2. Elsevier Inc., pp. 95–105. https://doi.org/10.1016/j.bpsgos.2021.08.005
Sato, M., Nakai, N., Fujima, S., Choe, K.Y., Takumi, T., 2023. Social circuits and their dysfunction in autism spectrum disorder. In: Molecular Psychiatry, Vol. 28(8. Springer Nature, pp. 3194–3206. https://doi.org/10.1038/s41380-023-02201-0.
Satterstrom, F.K., Kosmicki, J.A., Wang, J., Breen, M.S., De Rubeis, S., An, J.Y., Peng, M., Collins, R., Grove, J., Klei, L., Stevens, C., Reichert, J., Mulhern, M.S., Artomov, M., Gerges, S., Sheppard, B., Xu, X., Bhaduri, A., Norman, U., Buxbaum, J.D., 2020. Large-scale exome sequencing study implicates both developmental and functional changes in the neurobiology of autism. Cell 180 (3), 568–584.e23. https://doi.org/10.1016/j.cell.2019.12.036.
Schafer, D.P., Lehrman, E.K., Kautzman, A.G., Koyama, R., Mardinly, A.R., Yamasaki, R., Ransohoff, R.M., Greenberg, M.E., Barres, B.A., Stevens, B., 2012. Microglia sculpt postnatal neural circuits in an activity and complement-dependent manner. Neuron 74 (4), 691–705. https://doi.org/10.1016/j.neuron.2012.03.026.
Schafer, D.P., Lehrman, E.K., Heller, C.T., Stevens, B., 2014. An engulfment assay: a protocol to assess interactions between CNS phagocytes and neurons. J. Vis. Exp. 88 https://doi.org/10.3791/51482.
Schäfers, M., Sorkin, L., 2008. Effect of cytokines on neuronal excitability. Neurosci. Lett. 437 (3), 188–193. https://doi.org/10.1016/j.neulet.2008.03.052.
Schneider, H., Pitossi, F., Balschun, D., Wagner, A., Rey, A. Del, & Besedovsky, H. O. (1998). A neuromodulatory role of interleukin-1 in the hippocampus. In *Physiology* (Vol. 95). www.pnas.org.
Silverman, J.L., Turner, S.M., Barkan, C.L., Tolu, S.S., Saxena, R., Hung, A.Y., Sheng, M., Crawley, J.N., 2011. Sociability and motor functions in Shank1 mutant mice. Brain Res. 1380, 120–137. https://doi.org/10.1016/j.brainres.2010.09.026.
Spulber, S., Oprica, M., Bartfai, T., Winblad, B., Schultzberg, M., 2008. Blunted neurogenesis and gliosis due to transgenic overexpression of human soluble IL-1ra in the mouse. Eur. J. Neurosci. 27 (3), 549–558. https://doi.org/10.1111/j.1460-9568.2008.06050.x.
Spulber, S., Bartfai, T., Schultzberg, M., 2009. IL-1/IL-1ra balance in the brain revisited - evidence from transgenic mouse models. In Brain, Behavior, and Immunity (vol. 23 (5), 573–579. https://doi.org/10.1016/j.bbi.2009.02.015.
Spulber, S., Bartfai, T., Winblad, B., Schultzberg, M., 2011. Morphological and behavioral changes induced by transgenic overexpression of interleukin-1ra in the brain. J. Neurosci. Res. 89 (2), 142–152. https://doi.org/10.1002/jnr.22534.
Srinivasan, K., Friedman, B.A., Larson, J.L., Lauffer, B.E., Goldstein, L.D., Appling, L.L., Borneo, J., Poon, C., Ho, T., Cai, F., Steiner, P., Van Der Brug, M.P., Modrusan, Z., Kaminker, J.S., Hansen, D.V., 2016. Untangling the brain's neuroinflammatory and neurodegenerative transcriptional responses. Nat. Commun. 7 https://doi.org/10.1038/ncomms11295.
Stevens, B., Allen, N.J., Vazquez, L.E., Howell, G.R., Christopherson, K.S., Nouri, N., et al., 2007. The classical complement cascade mediates CNS synapse elimination. Cell 131 (6), 1164–1178. https://doi.org/10.1016/j.cell.2007.10.036.
Suzuki, K., Matsuzaki, H., Iwata, K., Kameno, Y., Shimmura, C., Kawai, S., Yoshihara, Y., Wakuda, T., Takebayashi, K., Takagai, S., Matsumoto, K., Tsuchiya, K.J., Iwata, Y., Nakamura, K., Tsujii, M., Sugiyama, T., Mori, N., 2011. Plasma cytokine profiles in subjects with high-functioning autism spectrum disorders. PLoS One 6 (5). https://doi.org/10.1371/journal.pone.0020470.
Takemiya, T., Fumizawa, K., Yamagata, K., Iwakura, Y., Kawakami, M., 2017. Brain interleukin-1 facilitates learning of a water maze spatial memory task in Young Mice. Front. Behav. Neurosci. 11 https://doi.org/10.3389/fnbeh.2017.00202.
Tang, G., Gudsnuk, K., Kuo, S.H., Cotrina, M.L., Rosoklija, G., Sosunov, A., Sonders, M.S., Kanter, E., Castagna, C., Yamamoto, A., Yue, Z., Arancio, O., Peterson, B.S., Champagne, F., Dwork, A.J., Goldman, J., Sulzer, D., 2014. Loss of mTOR-dependent macroautophagy causes autistic-like synaptic pruning deficits. Neuron 83 (5), 1131–1143. https://doi.org/10.1016/j.neuron.2014.07.040.
Terada, K., Yamada, J., Hayashi, Y., Wu, Z., Uchiyama, Y., Peters, C., Nakanishi, H., 2010. Involvement of cathepsin B in the processing and secretion of interleukin-1β in chromogranin a-stimulated microglia. Glia 58 (1), 114–124. https://doi.org/10.1002/glia.20906.

Thornton, P., McColl, B.W., Greenhalgh, A., Denes, A., Allan, S.M., Rothwell, N.J., 2010. Platelet interleukin-1α drives cerebrovascular inflammation. Blood 115 (17), 3632–3639. https://doi.org/10.1182/blood-2009-11-252643.

Tick, B., Bolton, P., Happé, F., Rutter, M., Rijsdijk, F., 2016. Heritability of autism spectrum disorders: A meta-analysis of twin studies. J. Child Psychol. Psychiatry 57 (5), 585–595. https://doi.org/10.1111/jcpp.12499.

Tomasoni, R., Morini, R., Lopez-Atalaya, J. P., Corradini, I., Canzi, A., Rasile, M., Mantovani, C., Pozzi, D., Garlanda, C., Mantovani, A., Menna, E., Barco, A., & Matteoli, M. (2017). *Lack of IL-1R8 in neurons causes hyperactivation of IL-1 receptor pathway and induces MECP2-dependent synaptic defects*. https://doi.org/10.7554/eLife.21735.001.

Tsai, P.T., Hull, C., Chu, Y., Greene-Colozzi, E., Sadowski, A.R., Leech, J.M., Steinberg, J., Crawley, J.N., Regehr, W.G., Sahin, M., 2012. Autistic-like behaviour and cerebellar dysfunction in Purkinje cell Tsc1 mutant mice. Nature 488 (7413), 647–651. https://doi.org/10.1038/nature11310.

Vargas, D.L., Nascimbene, C., Krishnan, C., Zimmerman, A.W., Pardo, C.A., 2005. Neuroglial activation and neuroinflammation in the brain of patients with autism. Ann. Neurol. 57 (1), 67–81. https://doi.org/10.1002/ana.20315.

Viviani, B., Gardoni, F., Marinovich, M., 2007. Cytokines and neuronal ion channels in health and disease. In International Review of Neurobiology (vol. 82, 247–263. https://doi.org/10.1016/S0074-7742(07)82013-7.

Walf, A.A., Frye, C.A., 2007. The use of the elevated plus maze as an assay of anxiety-related behavior in rodents. Nat. Protoc. 2 (2), 322–328. https://doi.org/10.1038/nprot.2007.44.

Wang, X., Tang, R., Wei, Z., Zhan, Y., Lu, J., Li, Z., 2023. The Enteric Nervous System Deficits in Autism Spectrum Disorder Vol. 17. https://doi.org/10.3389/fnins.2023.1101071.

Won, H., Mah, W., Kim, E., 2013. Autism spectrum disorder causes, mechanisms, and treatments: Focus on neuronal synapses. In Frontiers in Molecular Neuroscience (issue JULY). https://doi.org/10.3389/fnmol.2013.00019.

Wyszynski, R.W., Gibbs, B.F., Varani, L., Iannotta, D., Sumbayev, V.V., 2016. Interleukin-1 beta induces the expression and production of stem cell factor by epithelial cells: crucial involvement of the PI-3K/mTOR pathway and HIF-1 transcription complex. Cell. Mol. Immunol. 13 (1), 47–56. https://doi.org/10.1038/cmi.2014.113.

Xu, Z.X., Kim, G.H., Tan, J.W., Riso, A.E., Sun, Y., Xu, E.Y., Liao, G.Y., Xu, H., Lee, S.H., Do, N.Y., Lee, C.H., Clipperton-Allen, A.E., Kwon, S., Page, D.T., Lee, K.J., Xu, B., 2020. Elevated protein synthesis in microglia causes autism-like synaptic and behavioral aberrations. *Nature*. Communications 11 (1). https://doi.org/10.1038/s41467-020-15530-3.

Yan, J, Porch, MW, Court-Vazquez, B, Bennett, MVL, Zukin, RS, 2018. Activation of autophagy rescues synaptic and cognitive deficits in fragile X mice. Proc NatlAcad Sci USA 115 (41), E9707–E9716. https://doi.org/10.1073/pnas.1808247115.

Yi, F., Danko, T., Botelho, S.C., Patzke, C., Pak, C., Wernig, M., Südhof, T.C., 2016. Autism-associated SHANK3 haploinsufficiency causes Ih channelopathy in human neurons. Science 352 (6286). https://doi.org/10.1126/science.aaf2669.

Yirmiya, R., Winocur, G., Goshen, I., 2002. Brain interleukin-1 is involved in spatial memory and passive avoidance conditioning. Neurobiol. Learn. Mem. 78 (2), 379–389. https://doi.org/10.1006/nlme.2002.4072.

Yu, Y., Ozonoff, S., Miller, M., 2023. Assessment of Autism Spectrum Disorder. Assessment. https://doi.org/10.1177/10731911231173089.

Zhang, Y., Chen, K., Sloan, S.A., Bennett, M.L., Scholze, A.R., O'Keeffe, S., Phatnani, H.P., Guarnieri, P., Caneda, C., Ruderisch, N., Deng, S., Liddelow, S.A., Zhang, C., Daneman, R., Maniatis, T., Barres, B.A., Wu, J.Q., 2014. An RNA-sequencing transcriptome and splicing database of glia, neurons, and vascular cells of the cerebral cortex. J. Neurosci. 34 (36), 11929–11947. https://doi.org/10.1523/JNEUROSCI.1860-14.2014.

Zhao, H., Zhang, H., Liu, S., Luo, W., Jiang, Y., & Gao, J. (2021). Association of Peripheral Blood Levels of Cytokines With Autism Spectrum Disorder: A Meta-Analysis. In *Frontiers in Psychiatry* (Vol. 12). Frontiers Media S.A. https://doi.org/10.3389/fpsyt.2021.670200.

Zhou, Y., Kaiser, T., Monteiro, P., Zhang, X., Van der Goes, M.S., Wang, D., Barak, B., Zeng, M., Li, C., Lu, C., Wells, M., Amaya, A., Nguyen, S., Lewis, M., Sanjana, N., Zhou, Y., Zhang, M., Zhang, F., Fu, Z., Feng, G., 2016. Mice with Shank3 mutations associated with ASD and schizophrenia display both shared and distinct defects. Neuron 89 (1), 147–162. https://doi.org/10.1016/j.neuron.2015.11.023.